

T. Swift¹

Development of the Fail-safe Design Features of the DC-10

REFERENCE: Swift, T., "Development of the Fail-safe Design Features of the DC-10," *Damage Tolerance in Aircraft Structures, ASTM STP 486*, American Society for Testing and Materials, 1971, pp. 164-214.

ABSTRACT: The degree of damage tolerance used in the design of the DC-10 fuselage pressure shell is discussed with reasons for its selection. Analysis methods are presented for the prediction of the residual strength of damaged, stiffened panels, based on the matrix force solution of an idealized structure combined with fracture mechanics equations. The results of 20 different configurations are included. A description of the development test program to verify the analytical techniques and to substantiate the fail-safe strength of the fuselage shell is given together with the results for many of the tests.

KEY WORDS: airplanes, damage, tolerance (mechanics), aircraft panels, fuselages, reinforcement (structures), stiffening, cracking (fracturing), fatigue (materials), failure, fracture strength, axial stress, loads (forces), residual stresses, tests

With the introduction of wide-bodied jet transport such as the McDonnell Douglas DC-10, fail-safe design has become increasingly important, particularly in the pressurized fuselage shell. The radial loading due to pressure has increased dramatically since the introduction of the first pressure shell design. This paper presents some of the steps taken during the development phases to ensure a fail-safe fuselage design.

The DC-10 aircraft is designed for a life of 120,000 hours which, based on a scatter factor of 2, represents 60,000 crack-free hours or 20 years of service at 3000 flight hours per year [1].²

A more realistic review of damage tolerance was required in which areas where fatigue damage is more likely to occur were considered. Analysis methods which included the capability to vary the degree of damage were developed to determine the residual strength of damaged, stiffened structure. A self-propagating crack can be arrested in a region of low stress ahead of the crack tip by providing adequate circumferential and longitudinal stiffening. The crack tip stress is reduced as the load is redistributed into the

¹ Senior engineer scientist, Douglas Aircraft Co., McDonnell Douglas Corp., Long Beach, Calif. 90801.

² Italic numbers in brackets refer to the list of references at the end of this paper.

stiffeners. Various configurations were studied to produce an optimum structure, consistent with economy in manufacturing, which not only would provide fail-safe capability but also would improve the service life of the fuselage shell.

A comprehensive test program was initiated to verify the analytical method and to study various configurations and materials. Flat and curved panels were tested under uniaxial and biaxial loading, respectively. It was shown that, while flat panel testing is in many ways adequate from a qualitative viewpoint, certain secondary effects are present while others are neglected which should be accounted for in the determination of allowable stresses.

Damage Tolerance

The degree of damage to be tolerated in a pressurized fuselage shell, without catastrophic failure, is not specified completely in any of the requirements of the regulating agencies. The FAA requires that the structure shall be capable of sustaining damage amounting to a single principal structural element when subjected to the loading for the fail-safe conditions listed in section 25.571, part 25 of the Federal Aviation Regulations. However, owing to the large size of fuselage skin panels (approximately 400 by 80 in. for the DC-10), the single critical element normally is interpreted to mean one skin panel between any two longitudinal or circumferential stiffening members. This one-bay panel damage has been adopted by many designers in the past. To be realistic, however, one should consider how structural damage is initiated. Past experience has shown that the majority of damage incurred in service is due to fatigue, although isolated incidents such as engine cowls becoming detached, thrown engine parts, and small arms fire have been known to cause varying degrees of skin damage and should not be overlooked.

It was noted previously that the DC-10 is designed to be crack free for 60,000 hours (including scatter factors), which represents about 20 years of service; however, imperfections in manufacturing such as badly driven rivets which do not fill holes properly, the preloading of parts due to mismatch, and scratches received in service can reduce fatigue life, and thus the possibility of fatigue cracks occurring cannot be ignored.

Longitudinal Skin Cracks

Cabin pressurization is the main source of loading causing longitudinal skin cracks. Figure 1 shows that radial loading due to internal pressure on the DC-10 is $3\frac{1}{2}$ times as great as that for the DC-6, which was the first pressurized aircraft designed at Douglas. Testing on basic pressurized fuselage shell structure has indicated that longitudinal skin cracks are more likely to start in two critical locations, as follows:

1. Along the line of attachments which attach the outer fingers of a longitudinal splice member to the skin, as shown in Fig. 2: The radial tension stress due to pressure varies across a longitudinal skin bay and reaches a

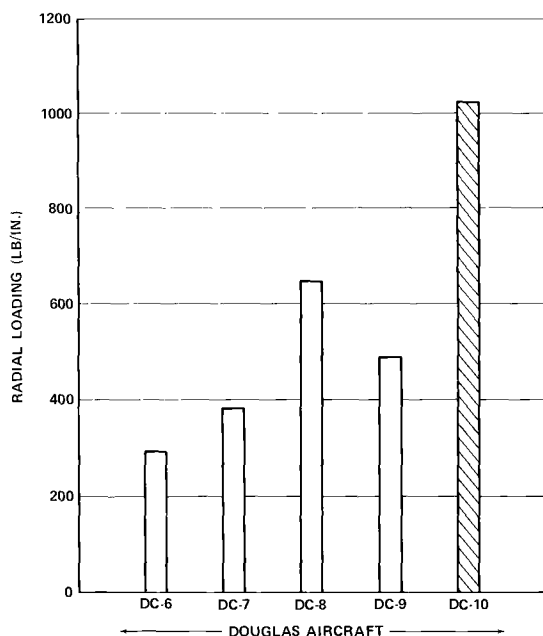


FIG. 1—Fuselage shell radial loading due to nominal cabin pressure.

maximum value midway between frames. Transfer of load from the skin into the finger doubler causes a high attachment bearing stress which, when combined with the radial tension stress, may cause a fatigue crack in a longitudinal direction. A large number of configurations for the longitudinal splice shown in Fig. 2 were fatigue tested. The configurations were changed until all failures occurred as shown in Fig. 2, where they can be detected by visual inspection methods. Fatigue cracks hidden by splice plates could propagate a considerable distance before detection.

2. At the first attachment of a frame shear clip to skin joint, as indicated in Fig. 3: The stress σ_c in the region of the shear clip cutout is higher than the midbay stress due to the discontinuity of the clip. In addition, the skin may be carrying tension stress due to frame bending. The high local stress, combined with the bearing stress in the first attachment hole as the shear clip picks up load, can cause a fatigue crack in the skin. The skin crack shown in Fig. 3a is just as likely to propagate into both adjacent bays as into one bay.

Transverse Skin Cracks

Testing under combined pressure and axial loads has indicated that transverse or circumferential skin cracks occur in two locations, as follows:

1. At the attachment of the skin to frame shear clip midway between longerons, as shown in Fig. 4: Local bending of the skin due to pressure, combined with axial stress due to fuselage bending, can cause skin cracks in a circumferential direction.

2. In the longeron flanges where they attach to the frame, as shown in Fig. 4: Bending due to transfer of some of the pressure loading into the frame increases the axial tension stress in the longeron flanges locally, causing fatigue cracks. After failure of the longerons, the skin stress increases locally (see Fig. 12) causing fatigue cracks in the skin which propagate into the two adjacent skin bays.

In view of the above facts, it is evident that damage extending to two skin bays should be considered. Materials and stress levels normally are chosen so that cyclic crack growth rates are low and a propagating crack will be noticed within a reasonable inspection period and before reaching a critical length; nonetheless, hairline cracks are extremely difficult to find under zero-load conditions and can easily escape detection. The design should, therefore, include the capability to arrest a crack after a fast fracture has occurred. The damage tolerance selected for the DC-10 fuselage shell was, therefore,

Two-bay longitudinal crack with the center frame intact

Two-bay circumferential crack with a center longeron failed

Configuration Candidates

The basic shell configuration selection is the result of many trade studies conducted to satisfy a number of requirements such as shell general instability, frame flexibility and strength, as well as fatigue and fail-safe strength. The results of these studies indicated that the frame spacing should be 20 in. and longeron spacing should vary from 8 in. at the top of the shell to 6.5 in. at the

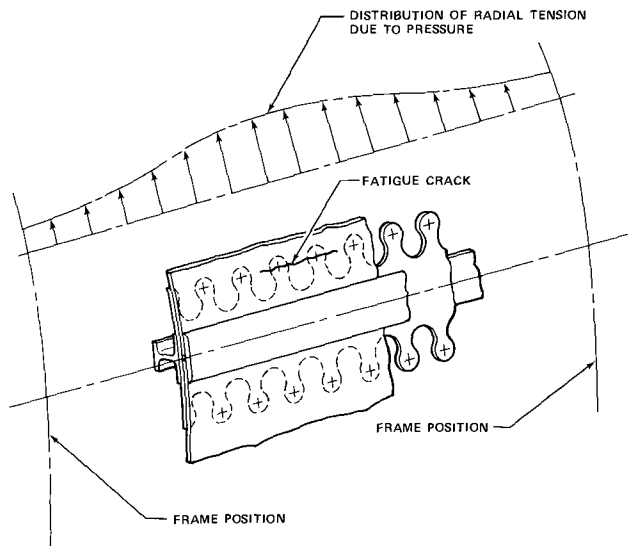


FIG. 2—Horizontal splice, fatigue crack location.

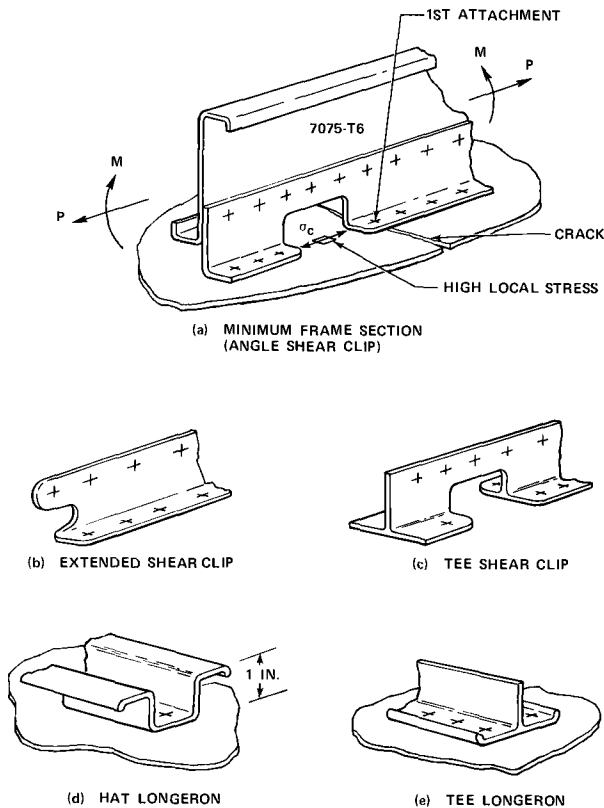


FIG. 3—Frame and longeron configurations.

bottom. The minimum bending stiffness of the frame section was set from general instability requirements. The outer and inner radii of the frame cross section were set by airplane performance and inside cabin dimension requirements, respectively. Although these basic dimensions were set for the minimum shell, several means were available to satisfy the fail-safe requirements to the damage tolerance specified. These were the selection of (a) skin thickness, (b) skin material, (c) whether or not to use crack stoppers, and (d) longeron geometric shape.

Skin Thickness

The skin thickness selection for the minimum gage portion of the fuselage is particularly important for an aircraft such as the DC-10. The surface area of the shell is approximately 8700 ft² with 84 percent of this minimum gage; one gage variation can thus represent a weight change of approximately 950 lb.

The most predominant loading condition for the minimum gage portion of the shell is due to pressurization. The fuselage is subjected to one full pressure cycle virtually every flight and, therefore, fatigue plays a vital part

in the selection of the minimum gage. Hoop tension stresses should be kept to reasonably low limits to prevent failures in horizontal splices and in longeron-to-skin rivet lines. It should also be noted that local bending stresses due to pressure, in areas such as those illustrated in Fig. 4, increase in inverse proportion to the skin thickness squared. Longitudinal crack propagation is decreased with decreasing hoop tension stress due to increasing skin thickness. Residual strength is increased to a lesser degree as will be illustrated later.

Skin Material

The skin material choice is perhaps the most important factor affecting the residual strength of a damaged fuselage shell. An independent research and development (IRAD) program on residual strength of stiffened flat wide panels [2] had resulted in the following values of plane stress fracture toughness K_{Ic} for four candidate materials: 52,700 to 63,500 $\text{psi}\sqrt{\text{in.}}$ for 7075-T6, 70,000 $\text{psi}\sqrt{\text{in.}}$ for 2014-T6, 90,000 $\text{psi}\sqrt{\text{in.}}$ for 7075-T73, and as high as 158,000 $\text{psi}\sqrt{\text{in.}}$ for 2024-T3. From a static strength standpoint, the ideal choice would be 7075-T6. In the past, 2014-T6 had been used successfully; but, in view of the increased radial loading (Fig. 1) and the tendency to work to higher stress levels [1], it was considered that a material with a higher fracture toughness would be more desirable. 7075-T73 and 2024-T3 were therefore considered as candidates.

Crack Stopper Straps

The use of crack stopper straps is an effective means of increasing the residual strength of damaged panels. An unstable fast fracture can be confined to a local area by providing an area of low stress ahead of the crack tip. The crack tip stress is reduced as a large part of the redistributed load is transferred into the strap. A region of low stress also can be provided, to a lesser degree, by a frame connected to the skin by shear clips as indicated in

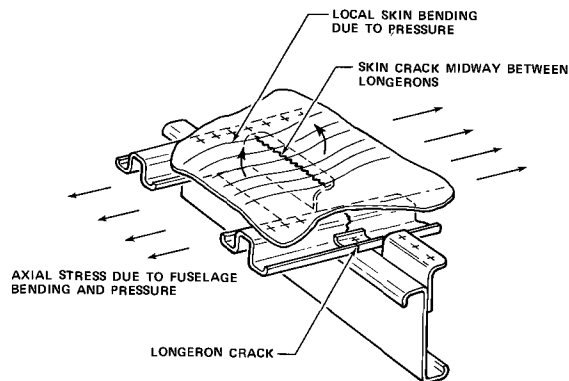


FIG. 4—Crack locations, fuselage shell.

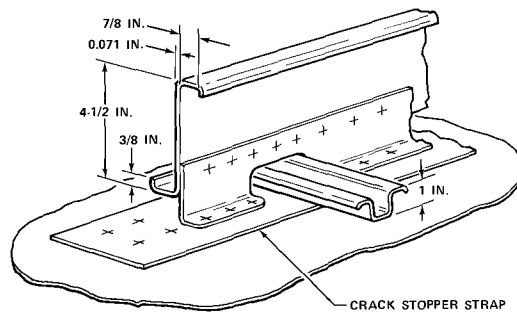


FIG. 5—Frame crack stopper configuration.

Fig. 3. The latter configuration would be desirable from a cost standpoint if the required residual strength could be attained.

When crack stopper straps are required, it has been Douglas policy to install them at a frame location, as illustrated by Fig. 5, for several good reasons. Without crack stopper straps, the skin stress level in the vicinity of the frames between shear clips (Fig. 3) has been determined both from flat panel and curved panel pressure tests to be up to 18 percent higher than the midbay hoop stress. With crack stopper straps to provide continuity across the gap, the stress level in this critical area is reduced to 15 percent below the midbay stress, thus reducing the possibility of a fatigue crack starting. In addition, the crack stopper strap can be used as bending material to increase the frame stiffness and static strength. Tests have shown that after cutting a 3-in.-long slot in the skin over a titanium crack stopper strap almost 14,000 cycles are required at 15,500-psi gross stress with a stress ratio $R = 0.05$ to fail the strap. During this number of cycles, crack propagation was negligible until the crack stopper had failed. Prior to failure of the crack stopper, the increase in frame stress due to the crack was negligible, thus reducing the possibility of frame fatigue failure. With the strap at any other location, the possibility of starting a crack in the skin is increased, and, once a crack started, propagation would be much faster and the possibility of failing the frame in fatigue would be increased.

There is one advantage in placing the crack stopper midway between frames for cracks which start at frames: the crack would be confined to 20 in. in length; however, with this configuration the crack is more likely to start. If a midbay crack stopper is installed by riveting, a crack is just as likely to start at a rivet hole and propagate both ways. Tests have shown that before a crack propagates very far, the crack stopper would fail in fatigue due to the high load transfer into the strap. In highly loaded areas the adjacent frames (without crack stoppers) would be incapable of arresting the crack. The outer crack stoppers would therefore be required to arrest a 40-in. crack without the help of a backup frame. The possibility of starting a crack at a midbay crack stopper would be reduced if the strap were bonded to the skin without

additional rivets. This configuration was considered for the DC-10 and abandoned for several reasons. The candidate material for crack stoppers was titanium and bonding of this material to aluminum was not considered as reliable as riveting. The bonding could easily become delaminated in service, especially under repeated shear loading of the skin panels and possible wrinkling due to tension field action. The longerons, passing over the bonded-on strap, would still require riveting through the strap. The bonding is subjected to delamination locally where the holes are drilled and the subsequent riveting operation is completed. Delaminations have been experienced where bonding is combined with riveting due to differences in the shear stiffness of the bonding material and the rivets. In addition, moisture seeping into the rivet holes and subsequently into the bonded surface has been known to cause delamination through corrosion.

Minimum weight structure with maximum reliability, consistent with the damage tolerance selected, was required. It also should be remembered that fatigue cracks, if they occur in service, usually form after many years of service. Techniques used to prevent rapid fracture should therefore be designed to perform other functions, for maximum economy, and yet be ready to stop a fast fracture without having deteriorated during service.

Another reason for abandonment of the bonding process, and possibly the most significant, is the distortion of the aluminum skin caused by thermal effects due to the difference in the coefficient of expansion of the titanium and the aluminum. A small test panel was fabricated as shown in Fig. 6 and a strap of 0.025-in.-thick titanium bonded to it and cured at a temperature of 250 F (121 C). On cooling to room temperature, the panel curved to approximately 70 in. in radius with the strap on the convex side. The panel was rolled to the correct radius with the strap on the concave side. The resulting

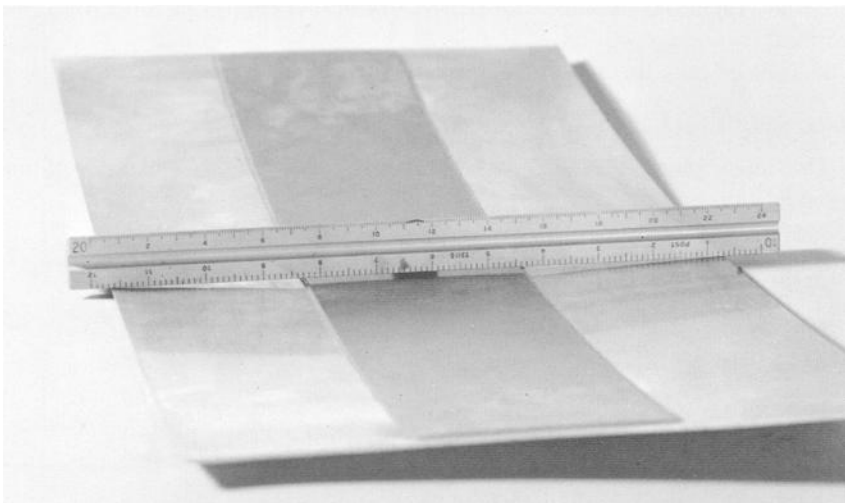


FIG. 6—Test panel distortion due to bonding process.

anticlastic curvature due to residual stresses is illustrated in Fig. 6. It was thought that this effect would be more severe on large panels, especially with longerons and frames assembled to the panels; the resulting quilted appearance of the shell would almost certainly be unacceptable to the customer.

Longeron Geometric Shape

Hat-section longerons such as those illustrated in Fig. 3d have been used on all previous Douglas aircraft. However, analysis indicated that for the damage tolerance selected for circumferential cracks, T-section longerons riveted to the skin with two rows of rivets would give higher allowable stresses. The hat-section longerons were desirable from a cost standpoint because of the cost of the extra row of rivets required in the T-section longerons. Both T- and hat-section longerons were therefore chosen as candidates. Analysis and test programs were introduced to study the configurations.

Analysis

Analysis of the candidate configurations for the damage tolerance selected was highly desirable prior to starting the development test program. In early work at Douglas [3, 4, 5] parametric lumped parameter analysis had been performed on 60-in.-wide panels with a single stiffening element containing a one-bay crack. Although this analysis proved to be extremely helpful in preliminary design work, further refinements were required to answer some of the questions listed below for panels containing two-bay cracks.

How effective was the frame member working in conjunction with a crack stopper strap?

How did the stress vary across the frame?

What effect did a broken longeron have on the crack tip stress for a circumferential crack and how did the stress vary across the outer longeron cross section?

In view of this, the analysis described herein was initiated.

Analysis of Cracked Unstiffened Panels

The most generally accepted equation for the fracture strength of unstiffened thin panels containing a central crack is

$$\sigma_R = \frac{K_c}{C\sqrt{W \tan \frac{\pi a_c}{W}}} \dots \dots \dots (1)$$

where

- σ_R = gross stress at failure,
- K_c = plane stress fracture toughness, psi $\sqrt{\text{in.}}$,
- C = width correction factor [7] $1.0 + 0.3 (2a/W)^2$,
- a_c = half crack length at fast fracture, and
- W = panel width.

For large panel widths, Eq 1 can be simplified as follows:

$$\sqrt{W \tan \frac{\pi a_c}{W}} = \left[\pi a_c + \frac{W}{3} \left(\frac{\pi a_c}{W} \right)^3 + \frac{2W}{15} \left(\frac{\pi a_c}{W} \right)^5 + \dots \right]^{1/2}$$

For large values of W then

$$\sqrt{W \tan \left(\frac{\pi a_c}{W} \right)} \rightarrow \sqrt{\pi a_c}$$

therefore Eq 1 reduces to

$$\sigma_R = \frac{K_c}{\sqrt{\pi a_c}} \dots \dots \dots (2)$$

Analysis of Cracked Stiffened Panels

The effects of stiffeners on the fracture strength of stiffened panels can be determined by a lumped parameter analysis of a structure representing the panel. The analysis is based on the matrix force method of structural analysis [8, 9] and uses the Fortran matrix abstraction technique (FORMAT) [10] to solve the matrix operations. Figures 7 and 8 show the idealized structure representing the stiffened panels for one- and two-bay longitudinal cracks, respectively. Figure 9 shows the idealized model for the two-bay circumferential crack. As illustrated, the panels are divided into a series of discrete bars and shear panels, the bars carry axial load and the panels carry shear load. The panels have the same thickness as the plate, and the bar areas are determined from the dimensions shown in Fig. 8 as follows:

$$A_y = t(z_1 + z_2)/2 \quad \text{and} \quad A_x = t(y_1 + y_2)/2$$

Loads are applied to the tops of the panels, and reactions are provided at the bottoms. The propagating crack is simulated by successive disconnection of the reactions in the skin at the horizontal center line of the panel by an element modification procedure which is part of the computer program. The crack tip stress is defined by the stress in the last bar adjacent to the simulated crack as shown in Fig. 7. The stiffening elements are represented by additional lumped bars connected to the main panel by a series of continuous shear panels.

A typical frame cross section with crack stopper strap is idealized by lumping areas as shown in Fig. 10. As the crack propagates in the skin, the frame outer cap picks up load through the shear clip-to-frame attachment row. The area of the outer cap, A_o , is therefore calculated so that its center of gravity (cg) lies on this attachment row. Frames without crack stoppers (see Fig. 3) are idealized by three lumped bars. The thickness of the idealized shear panels connecting the crack stopper and frame members to the skin is extremely important and is calculated to include the rivet stiffnesses.

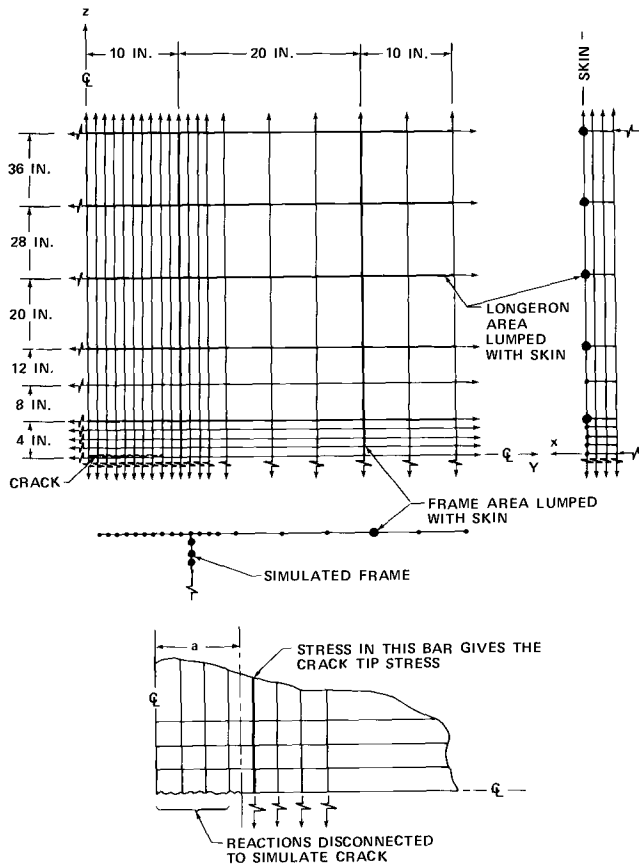


FIG. 7—Idealization for one-bay longitudinal crack.

Rivet shear deflection in aluminum alloy sheet is expressed as

$$\delta = \frac{Pf}{E_a d} \dots \dots \dots (3)$$

where

- δ = deflection,
- P = applied load,
- E_a = modulus of aluminum, and
- d = rivet diameter.

and, for aluminum alloy rivets,

$$f = 5.0 + 0.8 \left(\frac{d}{t_1} + \frac{d}{t_2} \right) \dots \dots \dots (4)$$

where t_1 and t_2 are the thicknesses of the joined sheets.

For the shear clip to crack stopper and skin to crack stopper rivets,

$$f = 5.0 + 0.8 \left(\frac{d}{t_1} + \frac{d}{t_2} \frac{E_a}{E_{cs}} \right) \dots \dots \dots (5)$$

where E_{cs} = modulus of crack stopper material.

These equations have been substantiated by test (see Fig. 26). The thickness of the idealized shear panels connecting the crack stopper to the skin is calculated as follows:

$$\text{Rivet deflection } \delta_r = \frac{Pf}{nE_a d}$$

where n = number of rivets between longerons.

$$\text{Idealized shear panel deflection } \delta_{csp} = \frac{Ph_{csp}}{Lt_{csp}G_a}$$

where L = distance between longerons and G_a = shear modulus of aluminum. However, $\delta_r = \delta_{csp}$, and equating deflections and solving for t_{csp} ,

$$t_{csp} = \frac{h_{csp}nE_a d}{LG_a f} \dots \dots \dots (6)$$

The shear clip is idealized in a similar manner including both rows of rivets and the sheet metal clip.

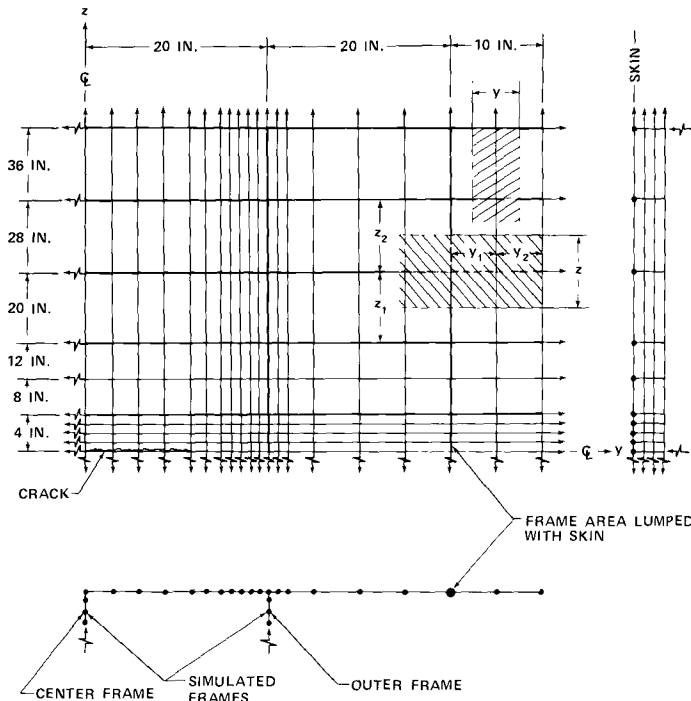


FIG. 8—Idealization for two-bay longitudinal crack.

For longitudinal bars located at longeron positions, the longeron area is included with the skin area in the plane of the sheet. Longerons in panels containing circumferential cracks are idealized into two lumped bars connected to the skin by a continuous shear panel. The thickness of the panel is determined using an equation similar to Eq 6.

The effect of stiffeners on the crack tip stress is determined by analyzing both unstiffened and stiffened panels having the same grid size and taking ratios between the crack tip stresses. The crack tip stress ratio, which is a function of crack length, is expressed as

$$R_{ct} = \frac{\sigma_{yct} \text{ in unstiffened panel}}{\sigma_{yct} \text{ in stiffened panel}}$$

where σ_{yct} is the stress in the y direction at the crack tip. Since Eqs 1 and 2 are directly related to the plate net stress in the region of the crack tip, they can be rewritten to include the effects of stiffening.

The presence of secondary effects [11] such as crack buckling makes the determination of K_c as a material parameter extremely difficult. K_c is, therefore, replaced by K_c^* which includes secondary effects; thus Eqs 1 and 2 become, for finite width panels,

$$\sigma_R = \frac{K_c^* R_{ct}}{C \sqrt{W \tan \frac{\pi a_c}{W}}} \dots \dots \dots (7)$$

and for infinite panels,

$$\sigma_R = \frac{K_c^* R_{ct}}{\sqrt{\pi a_c}} \dots \dots \dots (8)$$

K_c^* determined from tests on stiffened panels of one configuration can be used to determine the fracture strength of a fuselage shell of another configuration by using Eq 8, provided R_{ct} versus crack length has been determined. The use of R_{ct} , determined from analysis of a finite panel, can be justified for use in Eq 8 for an infinite plate if the panel is wide enough. A comparison of the net section stress for the panel of Fig. 7 to Westergaard's equation for the net section stress of an infinitely wide plate is shown in Fig. 11.

Analysis Results

Table 1 lists some of the more important analysis cases considered. Cases 1 to 9 and 10 to 12 are for two-bay and one-bay longitudinal cracks, respectively, where the frame members and circumferential crack stopper straps cause a reduction in crack tip stress. Cases 13 to 20 are for two-bay circumferential cracks with a broken central longeron, where the outer longerons cause a reduction in the crack tip stress. For all of the cases listed in Table 1,

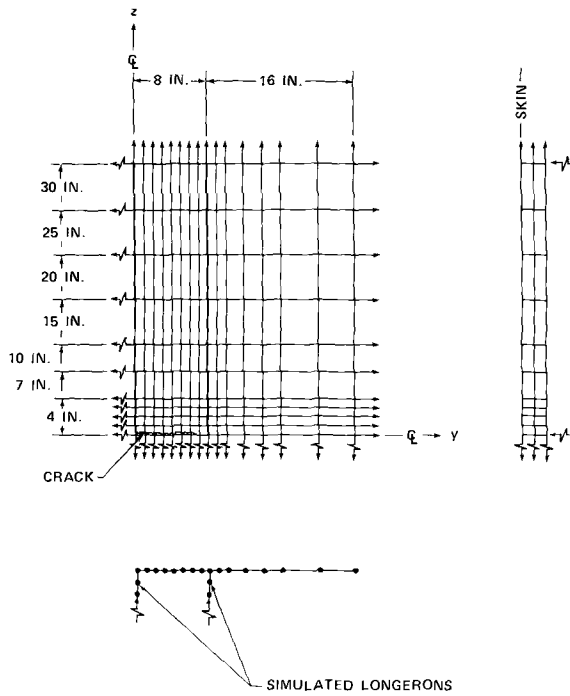


FIG. 9—Idealization for two-bay circumferential crack.

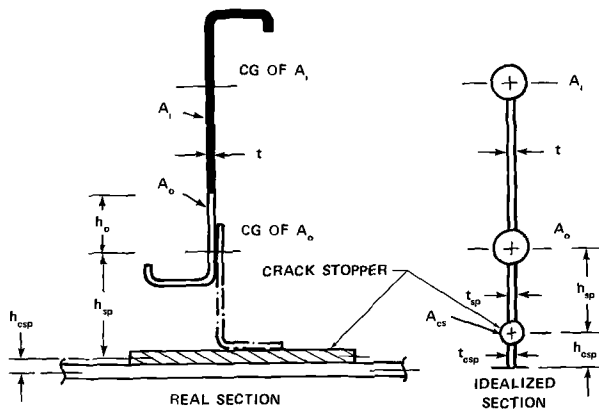


FIG. 10—Frame idealization with crack stopper.

a uniform stress level was applied to the upper boundary of the panels (shown in Figs. 7, 8, and 9) to both skin and stiffening elements. The results of the analysis cases considered are listed in Tables 2, 3, and 4. The frame cross sections for cases 1 to 12 and the hat sections for cases 13 to 18 are similar to those shown in Fig. 5. The stress ratio terms are defined below.

σ	Gross stress applied to the upper boundary of the panel, psi
σ_{ccs}	Center crack stopper stress, psi
σ_{ocs}	Outer crack stopper stress, psi
σ_{occf}	Outer cap stress in the center frame, psi
σ_{iccf}	Inner cap stress in the center frame, psi
σ_{ocof}	Outer cap stress in the outer frame, psi
σ_{icof}	Inner cap stress in the outer frame, psi
σ_{of}	Longeron outer fiber stress, psi
σ_{if}	Longeron inner fiber stress, psi

All of the stresses shown are lumped stresses in the idealized members. The stress distributions in the sheet after a longeron is broken and prior to skin cracking are shown in Fig. 12 for conditions 15 and 17 of Table 1.

Skin Fracture Criterion

The significance of Eqs 7 and 8 is illustrated in Fig. 13 and represents the residual strength of a panel, based on skin criteria. The lower curve (dotted) represents an unstiffened panel and the upper two curves are for stiffened panels with longitudinal cracks plotted for cases 1 and 4 of Table 1. The change in slope of the curves for stiffened panels as the crack tip approaches the stiffener spacing is due to a reduction in crack tip stress as the stiffener picks up load. The maximum reduction in crack tip stress occurs in the region of the stiffeners, as can be seen by the increase in R_{ct} values listed in Table 2.

If the panel contains a fatigue crack of half length a_A , and a gross stress of σ_{RA} is applied, then fast fracture will occur at A and the crack will be arrested at B . If, on the other hand, a gross stress of σ_{RC} is applied with half crack length equal to a_C , then fast fracture will occur at C and the crack will not be arrested. The residual strength of the panel is represented as σ_{RD} and any fracture at stress level higher than σ_{RD} will not be arrested and would represent an explosive failure in a pressurized shell. The value of the crack stoppers for case 4 can be seen by their influence on the residual strength when compared to case 1 for the panel without crack stoppers. The frame, connected to the skin by a flexible shear clip, is not as effective in picking up load as a crack stopper strap connected directly to the skin with three rows of rivets.

Stiffener Strength Criteria

In considering the gross residual strength of a stiffened panel, one must consider both skin fracture criteria and stiffener strength. Tables 2, 3, and 4

TABLE 1—Description of analysis cases.

Case No.	Case Description	Crack Type
1	Frames without crack stoppers; 0.071 skin; center frame intact	Two-bay longitudinal crack
2	Frames without crack stoppers; 0.080 skin; center frame intact	
3	Frame with crack stopper; 0.071 skin; crack stopper 3 by 0.025-in. titanium with three rows of 3/16 rivets; center crack stopper intact	
4	Same as case 3 with center crack stopper failed	
5	Same as case 3 with both center crack stopper and center frame failed	
6	Frame with crack stopper; 0.071 skin; crack stopper 2.8 by 0.025-in. titanium with two rows of 3/16 rivets; center crack stopper failed	
7	Frame with crack stopper; 0.071 skin; crack stopper 2 by 0.02-in. titanium with two rows of 3/16 rivets; center crack stopper failed	
8 ^a	Frame with crack stopper; 0.063 skin; crack stopper 3.25 by 0.016-in. titanium with two rows of 3/16 rivets; center crack stopper failed	
9	Same as case 8 with center frame failed	
10	Frames without crack stoppers; 0.071 skin	One-bay longitudinal crack
11	Frames without crack stoppers; 0.08 skin	
12	Frames with crack stopper; 0.071 skin; crack stopper 3 in. by 0.025-in. titanium with three rows of 3/16 rivets	
13	Rolled hat-section longeron; net area 0.205 in. ² ; 0.063 skin; one row of 3/16 rivets at 1¼ pitch	Two-bay circumferential crack with central longeron
14	Same as case 13 with 0.071 skin	
15	Extruded hat-section longeron; net area 0.3029 in. ² ; 0.071 skin; one row of 3/16 rivets at 1¼ pitch	
16	Same as case 15 with 0.080 skin	
17	Extruded hat-section longeron; net area 0.5121 in. ² ; 0.071 skin; one row of 3/16 rivets at 1¼ pitch	
18	Same as 17 with one row of 3/16 steel attachments at 1¼ pitch	
19	Extruded T-section longeron; net area 0.2895 in. ² ; two rows of 3/16 rivets at 1¼ pitch	
20	Extruded T-section longeron; net area 0.4865 in. ² ; two rows of 3/16 rivets at 1¼ pitch	

^a Case 8 frame thickness is 0.063 in. with dimensions as shown in Fig. 5.

list stiffener stresses as a function of crack length. To maintain the skin fracture strength illustrated by Fig. 13, the stiffeners must remain intact. In cases where the stiffener may be critical, yielding of the stiffener will take place prior to failure, resulting in an effective increase in the crack tip stress and a decrease in R_{ct} . Stiffener failure and skin fracture then occur simultaneously, but the failure is precipitated by stiffener criteria.

To obtain a balanced design, both skin and stiffener criteria must be considered, an example of which is illustrated in Fig. 14. The curves represent gross residual strength for a flat panel, stiffened by frames and crack stoppers and subjected to a uniform gross stress at the boundary. Curves are shown

TABLE 2—Stress ratios for two-bay longitudinal cracked panels.

Case	Half Crack Length, a , in.										
	4.5	7.5	10.5	12.75	15.5	17.5	18.5	19.5	20.5	21.5	
R_{et}											
1	1.100	1.160	1.220	1.270	1.350	1.435	1.500	1.615	1.750	1.810	
2	1.088	1.128	1.182	1.227	1.376	1.435	1.480	1.550	1.704	1.721	
3	1.260	1.317	1.392	1.446	1.540	1.651	1.758	2.171	2.908	2.786	
4	1.054	1.123	1.197	1.248	1.339	1.448	1.551	1.931	2.616	2.535	
5	0.777	0.824	0.867	0.896	0.954	1.033	1.112	1.402	1.940	1.923	
6	1.054	1.122	1.195	1.245	1.336	1.442	1.541	1.866	2.437	2.415	
7	1.075	...	1.207	1.255	1.341	1.438	1.523	1.785	2.268	2.266	
8	1.043	1.104	1.175	1.233	1.338	1.444	1.538	1.833	2.316	2.298	
9	0.769	...	0.851	...	0.952	1.027	1.099	1.324	1.701	1.724	
σ_{es}/σ	3	7.448	9.149	10.09	11.45	12.42	12.86	13.24	13.40	13.50	
σ_{os}/σ	3	1.727	1.777	1.874	2.243	2.698	3.185	4.266	6.364	7.354	
4	1.750	1.825	1.955	2.087	2.417	2.960	3.529	4.772	7.141	8.249	
5	1.858	1.994	2.229	2.451	2.994	3.844	4.695	6.499	9.804	11.33	
6	1.749	1.824	1.953	2.084	2.408	2.934	3.461	4.549	6.690	7.767	
7	1.745	...	1.943	2.073	2.408	2.985	3.621	5.103	8.640	10.44	
8	1.743	1.811	1.938	2.069	2.402	2.944	3.489	4.607	6.942	8.159	
9	1.841	...	2.190	...	2.955	3.802	4.625	6.259	9.549	11.252	
σ_{ect}/σ ...	1	1.643	2.104	2.576	3.261	3.566	3.710	3.845	3.956	4.050	
2	1.720	2.246	2.804	3.139	3.613	3.979	4.153	4.318	4.460	4.577	
3	1.251	1.447	1.658	1.782	1.965	2.099	2.160	2.213	2.235	2.251	
4	1.765	2.235	2.713	2.988	3.394	3.689	3.824	3.939	3.987	4.020	
6	1.760	2.224	2.696	2.969	3.372	3.665	3.800	3.916	3.972	4.011	
7	1.702	...	2.628	2.899	3.301	3.597	3.734	3.856	3.921	3.968	
8	1.672	2.113	2.574	2.884	3.245	3.538	3.674	3.792	3.855	3.899	

$\sigma_{\text{teof}}/\sigma_{\dots}$	1	0.966	1.019	1.117	1.192	1.317	1.420	1.471	1.519	1.561	1.596
	2	0.933	0.976	1.069	1.143	1.262	1.361	1.411	1.460	1.503	1.539
	3	1.024	1.092	1.189	1.256	1.364	1.449	1.489	1.524	1.539	1.550
	4	1.000	1.076	1.191	1.271	1.400	1.501	1.549	1.591	1.609	1.622
	6	1.001	1.078	1.193	1.273	1.403	1.505	1.553	1.596	1.617	1.632
	7	0.996	...	1.183	1.263	1.393	1.497	1.547	1.592	1.617	1.635
	8	0.981	1.041	1.136	1.206	1.322	1.414	1.459	1.499	1.521	1.537
$\sigma_{\text{ocof}}/\sigma_{\dots}$	1	1.022	1.057	1.119	1.176	1.304	1.470	1.596	1.781	2.082	2.325
	2	1.015	1.048	1.108	1.168	1.294	1.463	1.596	1.797	2.139	2.402
	3	1.013	1.036	1.077	1.118	1.208	1.321	1.402	1.505	1.579	1.634
	4	1.024	1.058	1.115	1.167	1.281	1.419	1.516	1.636	1.722	1.784
	5	1.073	1.136	1.239	1.329	1.523	1.750	1.904	2.091	2.217	2.306
	6	1.023	1.057	1.114	1.165	1.277	1.412	1.506	1.623	1.716	1.784
	7	1.022	...	1.113	1.166	1.282	1.427	1.531	1.666	1.790	1.882
	8	1.021	1.054	1.109	1.161	1.259	1.407	1.499	1.614	1.713	1.788
	9	1.069	...	1.228	...	1.509	1.731	1.879	2.059	2.206	2.316
$\sigma_{\text{teof}}/\sigma_{\dots}$	1	1.031	1.079	1.152	1.210	1.311	1.393	1.427	1.447	1.434	1.429
	2	1.025	1.070	1.144	1.204	1.308	1.396	1.434	1.457	1.437	1.430
	3	1.017	1.047	1.095	1.135	1.208	1.271	1.302	1.325	1.327	1.331
	4	1.032	1.077	1.144	1.197	1.292	1.374	1.413	1.443	1.447	1.453
	5	1.101	1.184	1.309	1.406	1.581	1.734	1.807	1.865	1.878	1.891
	6	1.032	1.076	1.114	1.196	1.291	1.374	1.413	1.445	1.453	1.461
	7	1.030	...	1.142	1.195	1.292	1.376	1.416	1.448	1.454	1.462
	8	1.029	1.070	1.134	1.184	1.275	1.352	1.389	1.419	1.425	1.433
	9	1.096	...	1.292	...	1.552	1.697	1.768	1.826	1.844	1.862

TABLE 3—Stress ratios for one-bay longitudinal cracked panels.

Case	Half Crack Length, a , in.										
	1.5	3.5	4.5	5.5	6.5	7.5	8.5	9.5	10.5	11.5	12.5
R_{ct}											
10	1.004	1.016	1.025	1.038	1.056	1.081	1.119	1.192	1.287	1.353	...
11	1.040	1.045	1.048	1.054	1.065	1.083	1.111	1.169	1.259	1.323	...
12	1.005	1.019	1.030	1.047	1.070	1.106	1.172	1.442	1.945	2.017	...
σ_{oss}/σ											
12	1.720	1.806	1.882	1.991	2.153	2.405	2.852	3.840	5.749	6.713	7.418
σ_{oocf}/σ ...											
10	1.009	1.046	1.076	1.118	1.174	1.249	1.353	1.509	1.765	1.989	2.183
11	1.008	1.045	1.074	1.117	1.174	1.253	1.364	1.533	1.819	2.066	2.281
12	1.008	1.040	1.067	1.103	1.149	1.210	1.289	1.389	1.462	1.518	1.571
σ_{icof}/σ ...											
10	1.008	1.040	1.064	1.093	1.125	1.159	1.191	1.214	1.209	1.210	1.217
11	1.008	1.040	1.065	1.095	1.130	1.167	1.203	1.228	1.217	1.217	1.224
12	1.007	1.036	1.058	1.085	1.116	1.150	1.184	1.213	1.218	1.225	1.235

TABLE 4—Stress ratios for two-bay circumferential cracked panels with broken central longeron.

Case	Half Crack Length, a , in.											
	1.5	2.5	3.5	4.5	5.5	6.5	7.5	8.5	9.5	11.0	13.0	
R_{et}												
13	0.818	0.853	0.881	0.907	0.937	0.980	1.101	1.327	1.394	
14	0.843	0.867	0.892	0.916	0.943	0.983	1.092	1.298	1.362	
15	0.778	0.820	0.852	0.883	0.918	0.970	1.107	1.353	1.428	
16	0.798	0.836	0.865	0.894	0.926	0.972	1.092	1.306	1.378	
17	0.683	0.736	0.779	0.822	0.871	0.942	1.124	1.428	1.520	
18	0.681	0.713	0.782	0.827	0.880	0.966	1.370	2.062	1.966	
19	0.763	0.813	0.851	0.886	0.926	0.988	1.201	1.593	1.646	
20	0.662	0.727	0.778	0.826	0.881	0.967	1.241	1.704	1.766	
$\sigma_{ot}/\sigma_{\dots}$												
13	1.066	1.107	1.172	1.270	1.425	1.694	2.247	3.504	4.304	5.436	6.451	
14	1.063	1.104	1.168	1.268	1.425	1.699	2.269	3.606	4.475	5.741	6.848	
15	1.074	1.114	1.176	1.269	1.414	1.660	2.153	3.212	3.875	4.805	5.606	
16	1.069	1.109	1.170	1.263	1.408	1.653	2.143	3.230	3.937	4.958	5.830	
17	1.094	1.132	1.189	1.271	1.394	1.591	1.955	2.637	3.043	3.601	4.052	
18	1.109	1.152	1.216	1.311	1.462	1.740	2.423	3.441	3.867	4.449	4.932	
19	1.077	1.121	1.186	1.280	1.420	1.649	2.089	2.864	3.290	3.890	4.412	
20	1.100	1.143	1.202	1.284	1.398	1.568	1.855	2.273	2.496	2.810	3.080	
$\sigma_{it}/\sigma_{\dots}$												
13	1.074	1.107	1.154	1.214	1.287	1.373	1.465	1.518	1.573	1.619	1.837	
14	1.070	1.103	1.149	1.209	1.284	1.372	1.466	1.520	1.579	1.705	1.863	
15	1.088	1.120	1.165	1.223	1.292	1.372	1.455	1.497	1.542	1.639	1.759	
16	1.082	1.114	1.159	1.217	1.287	1.369	1.454	1.501	1.551	1.659	1.793	
17	1.119	1.151	1.193	1.246	1.306	1.372	1.432	1.444	1.465	1.517	1.588	
18	1.124	1.158	1.203	1.257	1.320	1.384	1.422	1.377	1.371	1.387	1.427	
19	1.080	1.113	1.158	1.210	1.267	1.317	1.318	1.180	1.123	1.079	1.081	
20	1.108	1.141	1.180	1.221	1.257	1.268	1.201	0.982	0.881	0.772	0.715	

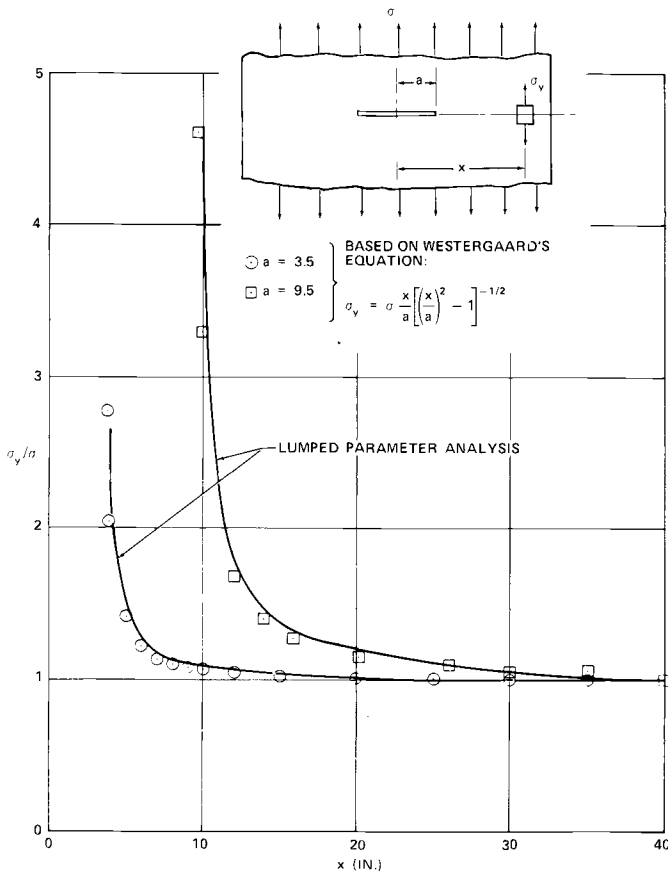


FIG. 11—Comparison of lumped parameter analysis with Westergaard's equation for infinitely wide plate.

for both skin fracture and center crack stopper criteria for case 3 of Table 1 where the center crack stopper is intact and for case 4 where the center crack stopper is broken. The skin material is assumed to be 7075-T73 with $K_{IC}^* = 90,000 \text{ psi } \sqrt{\text{in.}}$ [7]. The crack stopper and frame are assumed to be titanium 8-1-1 and 7075-T6, respectively, with ultimate tensile strengths of 149,000 and 75,000 psi. If the damage tolerance criteria selected require that the center crack stopper should not fail, then for a half crack length of 20 in. the gross strength would be limited to 11,000 psi from curve *A* of Fig. 14; however, the residual strength based on skin criteria is 31,500 psi from curve *B*, resulting in an unbalanced design. If, however, the center crack stopper is allowed to break, leaving the frame intact, the strength based on skin criteria would be reduced to 30,000 psi from curve *D*. The residual strength of the panel would be 19,000 psi for a half crack length of 20 in. based on center frame criteria. This is a case where increasing the damage tolerance would

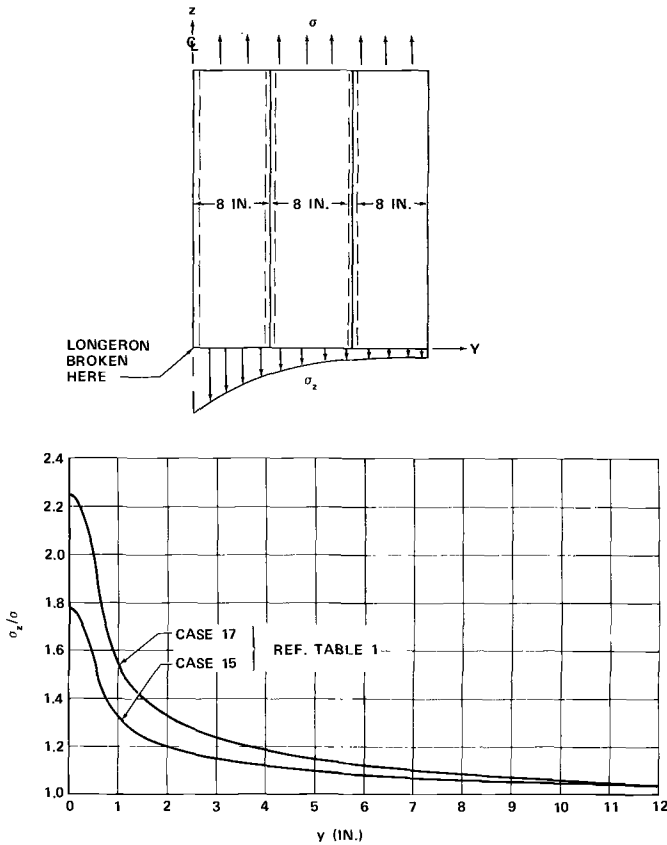


FIG. 12—Axial skin stress in the vicinity of a broken longeron.

reduce the weight, since the area of the crack stoppers would have to be more than doubled to maintain their continuity at a gross stress of 19,000 psi. The rivets attaching the crack stopper to the skin become highly loaded as the crack extends. Figure 15 shows outer crack stopper total rivet load as a function of crack length for cases 3, 4, and 6 of Table 1. Only the first and second rows are shown. For case 3, the rivets attaching the center crack stopper to the skin are extremely highly loaded analytically: for $a = 21.5$, P_r/σ is 0.348.

Test Program

Extensive fatigue and fail-safe testing had been completed during the development of the DC-8 and DC-9 aircraft. The general philosophy during the DC-8 testing was to subject a panel or shell structure to pressure loading which would simulate a principal stress in the skin. Rotary saws were then

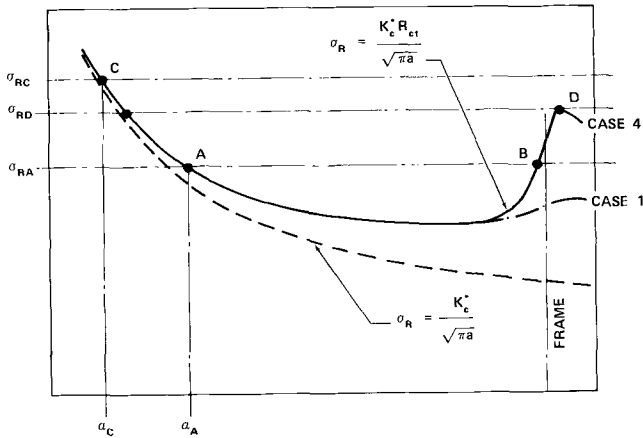


FIG. 13—Comparison of gross residual strength curves for unstiffened and stiffened panels, cases 1 and 4 of Table 1.

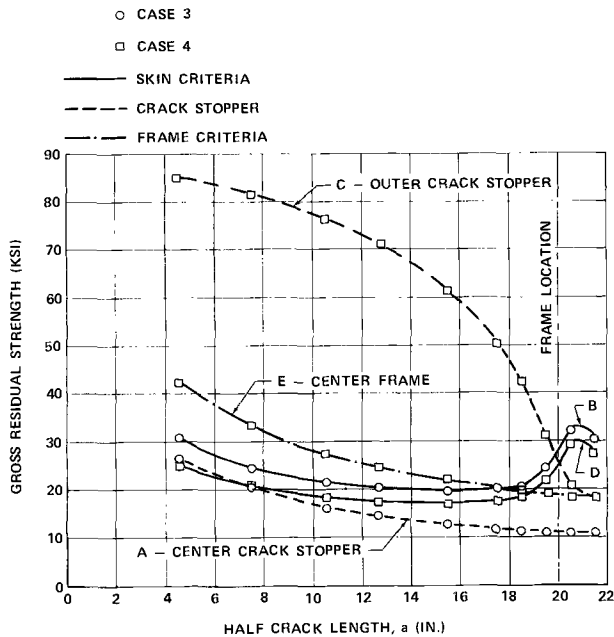


FIG. 14—Gross residual strength for a typical flat panel with two-bay longitudinal crack.

inserted into the skin and advanced until rapid fracture occurred. This method is excellent for determining the crack arresting capability of the crack barriers, but little information on fracture toughness is gained that can be used in future designs.

The methods changed during the DC-9 testing, where saw cuts were made in the skin and cyclic pressure applied so that the saw cuts were converted to fatigue cracks prior to fast fracture. Fracture toughness can be determined from this type of testing if the crack length at fast fracture is known. All of these early data were extremely useful during the development of the DC-10 fail-safe capability; nevertheless, in order to produce the most efficient design, further development testing was required. Figure 16 illustrates some of the fail-safe development test specimens completed to date.

Curved Panels

Figure 16a shows a large curved panel of 118.5-in. radius which is stiffened by eight frames and eleven longerons. Axial loading is applied by a series of whiffletrees attached to the ends of the panel. Pressure loading is applied to the underside of the panel by lowering a vacuum chamber onto the panel and evacuating the chamber. Both axial load and pressure loading can be cycled or applied statically. Transverse and longitudinal saw cuts can be made in the

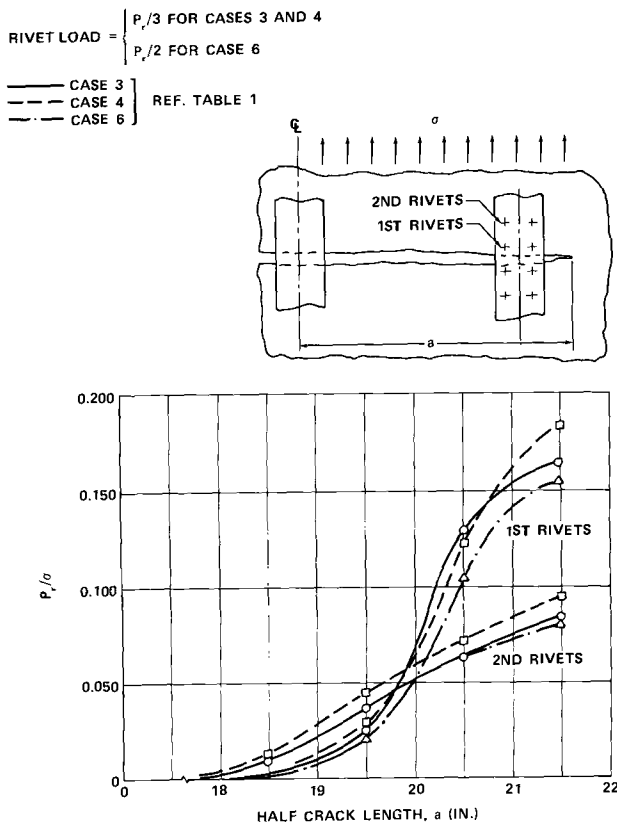


FIG. 15—Rivet shear load, outer crack stopper to skin rivets.

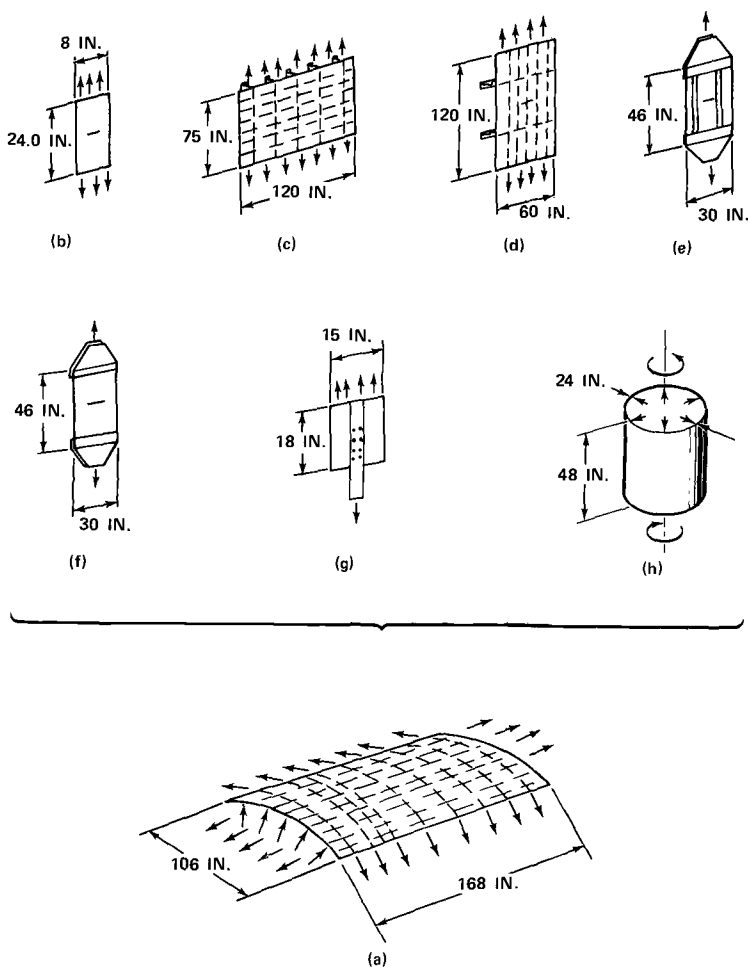


FIG. 16—Fuselage fatigue and fail-safe development tests.

skin and propagated into fatigue cracks prior to applying static loading to determine the effects of fast fracture and arrest.

The vacuum test machine was initiated during the DC-10 development and considerable effort was required to perfect its operation. The main innovations in this machine are the capability to apply axial load and the ability to observe the inner side of the panel during pressure loading. One circumferential and six longitudinal crack tests have been performed on two panels to date. Panel 15 was made from 0.080-in. 7075-T73 clad sheet, with a frame configuration as shown in Fig. 3a with a net area of 0.5042 in.². Longerons were extruded hat as seen in Fig. 3d with a gross area of 0.312 in.². Panel 16 was made from 0.063-in. 2024-T3 clad sheet with frame configuration as shown in Fig. 5 but of 0.063-in. thickness and 0.425-in.² net area. Crack

stoppers were 3.25 by 0.016-in. titanium 8-1-1 and longerons were rolled hat section with a gross area of 0.214 in.². During the development of the vacuum test machine shown in Fig. 17, all of the specimen types *b* to *g* of Fig. 16 were tested to give early data to be incorporated into the larger curved panels. A view of the upper side of curved panel 16 is shown in Fig. 18.

Figure 16*b* shows narrow specimens for material screening. Crack propagation and residual strength tests were performed on these specimens, but the fracture toughness data obtained are not representative of wide panels such as fuselage panels. This is illustrated by Liu [13] who shows the increase in plane stress fracture toughness K_{Ic} with increasing panel width. This effect is particularly noticeable in 2024-T3 sheet.

Flat Panels with Longitudinal Cracks

Figure 16*c* shows flat panels stiffened by longerons and frames. Fourteen tests were performed on six panels of this type. Frames on each of the panels were 7075-T6 with cross sections as shown in Fig. 3. Longerons were all 7075-T6 extruded hat section with a gross area of 0.312 in.². A description of the panel is given in Table 5. Three-inch-wide titanium crack stoppers 0.025 in. thick were incorporated into panels 5 and 6 with three rows of rivets. Cracks were propagated under uniaxial cyclic loading from saw cuts in the skin to simulate one-and two-bay longitudinal cracks. Static loading was applied at predetermined crack lengths to fast fracture the skin. Cracks were normal to the frames and crack stoppers provided the crack barriers.

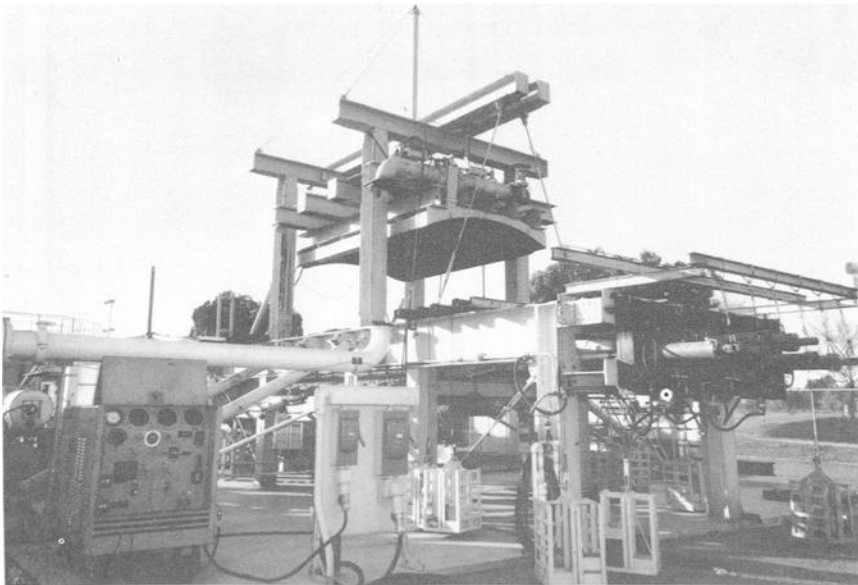


FIG. 17—Vacuum test rig for testing curved panels under combined pressure and axial loading.



FIG. 18—Upper side of curved test panel 16.

TABLE 5—120-in.-wide flat panel configuration for longitudinal cracks (frame spacing 20.0 in., skin thickness 0.071 in.).

Panel No.	Skin Material	Longeron Spacing, in.	Crack Stopper	Shear Clip Type ^a
1.....	7075-T73	6.5	None	(a)
2.....	7075-T73	8.0	None	(b)
3.....	7075-T73	6.5	None	(c)
4.....	7075-T73	8.0	None	(a)
5.....	7075-T73	8.0	3 by 0.025-in. titanium 8-1-1	(a)
6.....	2024-T3	8.0	3 by 0.025-in. titanium 8-1-1	(a)

^a Refer to Fig. 3.

Flat Panels with Circumferential Cracks

Figure 16*d* shows flat panels stiffened by longerons and frames. Eighteen tests were performed on nine panels of this type. The configurations of eight of these panels, listed from 7 to 14, are shown in Table 6. Longerons were saw cut, and cracks propagated into two adjacent bays under uniaxial cyclic loading to simulate a two-bay circumferential crack with a broken central

TABLE 6—60-in.-wide flat panel configuration for circumferential cracks (longeron spacing 8.0 in., skin thickness 0.071 in.).

Panel No.	Skin Material	Longeron Type ^a	Longeron Net Area, in. ²	Longeron to Skin Attachments
7.....	7075-T73	Hat (<i>d</i>)	0.3029	NAS 1097 DD6
8.....	7075-T73	Hat (<i>d</i>)	0.5121	NAS 1097 DD6
9.....	7075-T73	T (<i>e</i>)	0.2895	RV 5176-6 7075-T73
10.....	7075-T73	T (<i>e</i>)	0.4865	NAS 1097 DD6
11.....	2024-T3	Hat (<i>d</i>)	0.3029	NAS 1097 DD6
12.....	2024-T3	Hat (<i>d</i>)	0.5121	NAS 1097 DD6
13.....	2024-T3	T (<i>e</i>)	0.2895	RV 5170-6 7075-T73
14.....	2024-T3	T (<i>e</i>)	0.4865	RV-5170-6 7075-T73

^a Refer to Fig. 3.

longeron. At predetermined crack lengths, static loads were applied to fast fracture the skin. Cracks were normal to the longeron so that the longerons acted as crack barriers.

Figure 16e shows flat panels stiffened by crack stopper straps. Six panels of this type were tested, made from 0.071-in. 2024-T3 sheet with straps of various widths and thicknesses spaced 10 in. apart. The results of the two large flat panels with crack stoppers had indicated that perhaps two rivet rows were adequate, but, in view of the high rivet loads predicted by the analysis (Fig. 15), tests were needed to determine if the required load could be transferred without rivet failure. Nine-inch-long saw cuts were made in the skin with 1/8-in.-diameter holes drilled at the ends of the saw cut to delay any tendency to fast fracture the skin. Rivet edge distances were also varied, since the large flat panels had indicated the crack stoppers to be loaded more highly on the side from which the crack was approaching. Increasing edge distance would reduce the tendency to overload one side of the strap. Static loads were applied to failure in all of the tests. Loads input to the straps was measured by strain gages. Antibuckling guides were used on these tests.

Figure 16f shows 30-in.-wide unstiffened panels loaded uniaxially. During the early testing on the DC-8 where saw cuts were used, fracture toughness had been determined for 2024-T3 where the fracture had been initiated by a saw cut. Predictions were that for this material no difference would exist between fracture from a saw cut and fracture from a fatigue crack [14]. Two panels were tested for residual strength, one with a saw cut 9 in. long and the other with the same length of fatigue crack.

Figure 16g shows one of five small panels which had been cut from the fractured panels shown in Fig. 16e. The purpose of these panels was to determine the crack stopper to skin rivet shear load. Analysis had shown that the first rivets in the vicinity of the crack were highly loaded, and the possibility existed that these rivets could yield and redistribute load to the rivets away from the crack. Strain gages were installed between rivets and the load applied to the strap to failure. These panels were intended to simulate the case where the crack had propagated beyond the crack stopper.

Figure 16h shows one of 16 small, unstiffened cylinders 24 in. in diameter and 48 in. long made from 0.032 2024-T3 sheet. The purpose of these tests was to assess qualitatively the effects of shear and axial compression combined with pressure. The setup for testing the cylinders is illustrated in Fig. 19. An internal pressure source was provided by water and compressed air. Torque loading, applied to the top of the cylinders, was provided by two servo-controlled hydraulic jacks. The system was capable of applying cyclic or static pressure and torque loading simultaneously. Both torque and pressure loading were monitored and recorded using oscillograph instrumentation. Axial constraint was provided on some of the cylinders by using long steel bolts to hold the two end flanges together. Relief to the axial tensile stress due to pressure or the application of axial compressive stress was provided. Rosette strain gages located on the cylinders were monitored continuously by oscillograph recorders. Longitudinal fatigue cracks, initiated from saw cuts, were propagated to predetermined lengths by cyclic pressure loading. The test procedure subsequent to this operation is listed in Table 7.

TABLE 7--*Test procedure for 24-in.-diameter unstiffened cylinder test.*

Cylinder Number	Test Procedure
1	Cycle pressure loading until failure.
2	Increase pressure in increments to failure.
3	
4	
5	Increase torque and pressure in increments to failure, torque:pres-
6	sure ratio = 7750 in. ³
7	
8	Increase pressure to stabilize the cylinder. Tighten down the tie bolts
9	to provide axial constraint. Increase pressure to failure.
10	
11	
12	Hold pressure constant. Cyclic torque applied from zero to a torque:
13	pressure ratio of 7750 in. ³ until failure.
14	
15	Increase pressure to stabilize the cylinder. Increase torque to a con-
16	stant value. Cycle the pressure between 6.5 psi and 13.85 psi for
	cylinder 15 and between 9.0 psi and 21 psi for cylinder 16.

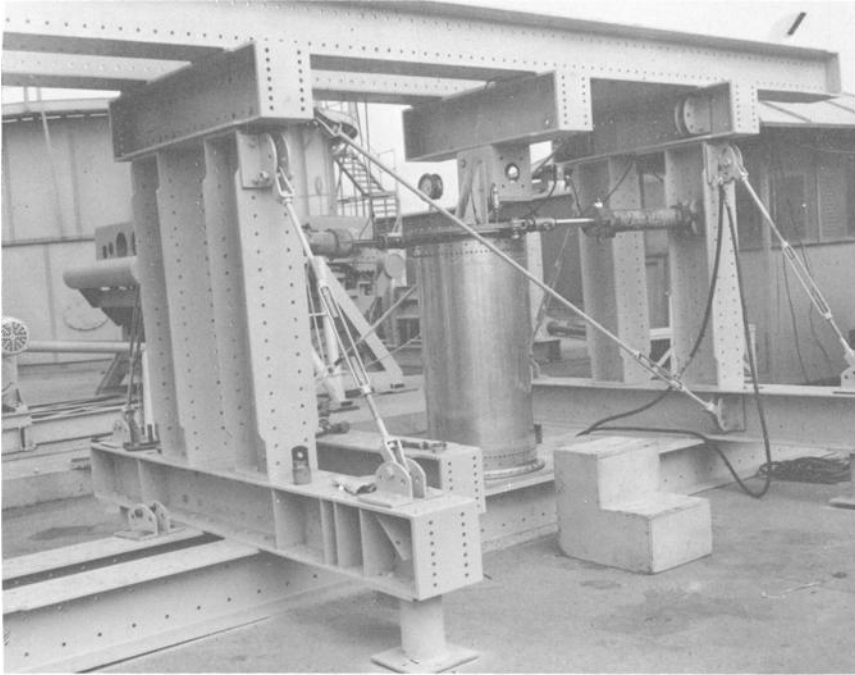


FIG. 19—Test fixture for 24-in.-diameter cylinders.

Test Results

Flat Panels with Longitudinal Cracks

The results of tests on the 120-in.-wide flat panels are shown in Table 8. Symbols not yet defined and used in the tables are

- a_{aC} Half crack length at crack arrest from calculation
- a_{FC} Half crack length at failure from calculation
- σ_{RC} Gross stress at failure from calculation

Test values are the same with the subscript T replacing the subscript C. Fracture toughness K_{IC}^* , listed for panels 1 and 2 tests 1 and 2, panel 3 test 1, and the first part of test 2 on panel 6, is the maximum value applied without fast fracture at the most critical crack length. For the two-bay tests on panels 2 and 5, the frame, central to the crack, was reinforced locally so that frame failure would not interfere with the skin critical criteria. Analysis had indicated (see Table 2) that the frame could fail prior to the skin and this was substantiated very accurately by the strain gages on panel 4. Analyses were performed to account for the reinforcing so that accurate R_{ct} values shown in Table 8 were available to determine K_{IC}^* . Final failure of panels 1, 2, 3, 4, and 6 was due to skin fast fracture during static loading. In all cases where cracks had terminated in rivet holes, cyclic loading was applied to restart a fatigue

TABLE 8—Test results for 120-in.-wide flat panels with longitudinal crack (panels 1 to 5, 0.071-in. 7075-T73 material; panel 6, 0.071-in. 2024-T3 material; all cracks parallel to grain).

Panel No.	Test No.	Gross Stress, psi	Half Critical Crack Length, in.	R_{ct}	C	K_{c}^*	Calculated			Test			Test/Calculated		
							a_{ac} , in.	a_{FC} , in.	σ_{RC} at Failure	a_{sT} , in.	a_{FT} , in.	σ_{RT} at Failure	a_{sT}/a_{sC} , in.	a_{FT}/a_{FC} , in.	σ_{RT}/σ_{RC} , in.
1.....	1 ^a	19 410	8.90	1.145	1.006	> 91 000
	2 ^a	19 410	8.90	1.145	1.006	> 91 000
2.....	1 ^a	22 000	8.90	1.145	1.006	> 103 137
	2 ^a	20 888	8.90	1.145	1.006	> 97 929
	3 ^b	17 300	16.60	1.430	1.023	92 000	18.30	21.50	19 000	19.63	21.48	18.476	1.072	0.999	0.972
3.....	1 ^a	19 410	8.90	1.145	1.006	> 91 000
	2 ^b	19 124	12.05	1.250	1.012	96 200	20.08	21.0	19 700	20.08	20.46	19.744	1.0	0.974	1.002
4.....	2 ^b	17 000	17.50	1.435	1.0255	93 400	18.63	21.50	19 000	19.63	20.97	18 100	1.054	0.975	0.953
	2 ^b	20 138	10.285	1.710	1.0085	95 700	19.0	20.40	24 994	19.00	20.40	25 118	1.0	1.0	1.004
6.....	2 ^b	19 000	16.325	0.98	1.0222	> 145 500
	2 ^b	20 000	21.875	1.26	1.040	145 500	21 875	20 000

^a One-bay crack.^b Two-bay crack.



FIG. 20—Arrest of two-bay longitudinal crack after fast fracture, test 2, panel 3.

crack. Final failure of panel 5 was due to outer crack stopper failure. Test 2 was performed on panel 6 with the center frame completely saw cut, and final failure occurred with center frame, center crack stopper, and one outer crack stopper failed. Figure 20 shows the crack arrestment after fast fracture on panel 3. The fail-safe value of the separate shear clip frame configuration is illustrated by the crack in the clip leaving the main frame intact. If the frames had been designed such that the clip were part of the main frame member, the crack would have propagated through the frame.

Flat Panels with Circumferential Cracks

The results of tests on the 60-in.-wide panels are shown in Tables 9 and 10. K_{e}^{*} values listed for panels 7 to 10 and for test 2 of panel 11 are determined at fast fracture from a two-bay crack with saw cut central longeron. The other K_{e}^{*} values listed are the maximum values applied without fast fracture at the most critical crack length. During test 2 of panels 11, 13, and 14, the maximum value of residual strength required for the aircraft had been applied without failure. In order to obtain data for a higher degree of damage, two longerons were saw cut so that failure occurred with three bays of skin and

TABLE 9—Test results for 60-in.-wide flat panels with circumferential crack (0.071-in. 7075-T73 skin material; cracks transverse to grain).

Panel No.	Test No.	Gross Stress, psi	Half Critical Crack Length, in.	R_{et}	C'	K_{σ}^*	Calculated			Test			Test/Calculated	
							$a_{\sigma C}$, in.	a_{FC} , in.	σ_{RC} at Failure	$a_{\sigma T}$, in.	a_{FT} , in.	σ_{RT} at Failure	$a_{\sigma T}/a_{\sigma C}$, in.	a_{FT}/a_{FC} , in.
7	1	25 160	4.040	0.870	1.0054	104 358	8.100	8.095	0.999	...
	2	26 540	4.123	0.875	1.0057	110 627	8.100	9.000	30 100	7.888	8.155	31 200	0.949	0.906
8	1	23 060	3.275	0.770	1.0036	97 350	7.750	7.675	0.990	...
	2	23 100	3.625	0.780	1.0044	100 942	7.600	8.900	28 700	7.600	8.350	29 600	1.000	0.938
9	1	23 100	3.500	0.850	1.0128	91 760	7.700	7.375	0.958	...
	2	28 600	2.440	0.810	1.0020	98 213	8.250	9.000	29 600	7.600	9.140	29 600	0.921	1.015
10	1	24 000	1.860	0.685	1.0012	84 973	7.900	7.265
	2	24 800	1.605	0.670	1.0009	83 318	8.200	8.810	27 500	7.560	8.810	27 800 ^a	0.921	1.000

^a Fast fracture to next longeron. Final failure at a gross stress of 36,052 psi with a total crack length of 32.67 in. and one broken longeron.

TABLE 10—Test results for 60-in.-wide flat panels with circumferential cracks (0.071-in. 2024-T3 skin material; cracks transverse to grain).

Panel No.	Test No.	Gross Stress, psi	Half Critical Crack Length, in.	R_{et}	C	K_c^*	Comments
11....	1	34 000	6.500	0.97	1.0141	>164 284	Final failure at gross stress of 27,921 psi with crack length of 25.69 in. equally spaced about two saw cut longerons
	2	40 000	6.205	0.95	1.0128	192 432	
12....	1	29 800	6.200	0.92	1.0128	>147 869	Final failure at gross stress of 40,855 psi with total crack length of 20.3 in. and one central saw cut longeron
	2	34 000	6.200	0.92	1.0128	>168 631	
13....	1	39 800	5.825	0.94	1.0113	>186 079	Final failure at gross stress of 30,966 psi with total crack length of 23.0 in. equally spaced about two saw cut longerons
	2	40 000	6.020	0.95	1.0121	>188 250	
14....	1	34 000	6.100	0.92	1.0124	>166 034	Final failure at gross stress of 34,293 psi with total crack length of 22.66 in. equally spaced about two saw cut longerons
	2	40 000	6.100	0.92	1.0124	>195 393	

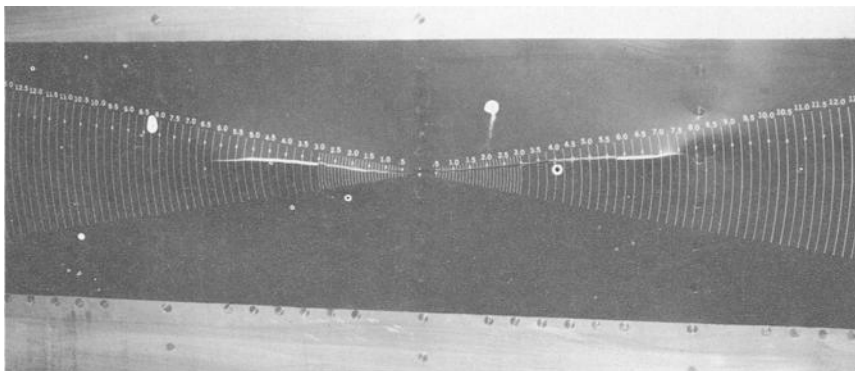


FIG. 21—Arrest of crack after fast fracture at gross stress of 39,931 psi, panel 11, test 2.

two cut longerons. The results of these tests are shown in Table 10. Figure 21 shows the crack arrestment during test 2 of panel 11; Fig. 22 shows the panel after final failure from a three-bay crack with two cut longerons.

Curved Panels

The test results for curved panels 15 and 16 are listed in Table 11. Four tests were completed on panel 15. Saw cuts were made in the skin in a longitudinal direction, 1 in. away from a longeron in all cases. Cracks were propagated to predetermined lengths under cyclic loading and static load was applied to cause fast fracture. The skin stresses are functions of both pressure P and axial load per inch of length N_x due to Poisson's ratio effects of the biaxially loaded skin. The equations governing the stresses are determined using the methods of Flugge [15]. Tests 1 and 3 were performed with pressure load only while axial load was present in the case of tests 2 and 4. Fast fracture of the cracks occurred for all tests on panel 15 and in each case the cracks

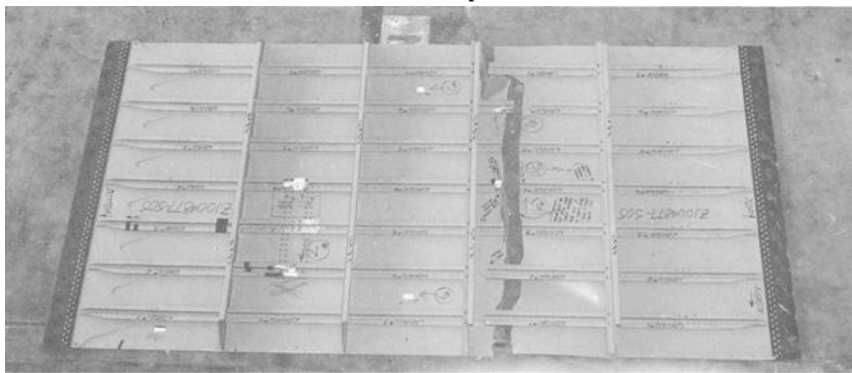


FIG. 22—Failure of panel 11 at gross stress of 27,920 psi from three-bay crack with two cut longerons.

TABLE 11—Test results for longitudinal crack tests on curved panels (panel 15 0.080-in. 7075-T73, panel 16 0.063-in. 2024-T3).

Panel No.	Test No.	P^a psi	$\sigma_{h_s}^b$ psi	$\sigma_{x_s}^c$ psi	$a_{e_s}^d$ in.	R_{e_t}	C	$K^* \frac{1}{\text{psi} \sqrt{\text{in.}}}$	Calculated			$\frac{a_{oT}}{a_{oC}}$	Analysis Case f
									σ_{RC}^e psi	a_{oC} in.	a_{oT} in.		
15. . . .	1 ^g	12.8	14 912	0	7.235	1.076	1.0023	66 460	14 750	10.60	10.06	0.95	11
	2 ^g	13.36	15 622	2 500	8.050	1.095	1.0028	72 000	16 000	10.06	10.06	1.0	11
	3 ^h	10.80	12 600	0	12.10	1.210	1.0064	65 114	13 300	19.60	19.88	1.014	2
	4 ^h	11.55	15 380	28 495	12.825	1.230	1.0072	80 573	16 500	19.50	19.88	1.019	2
16. . . .	1 ⁱ	12.1 ^k	16 700	0	13.148	1.240	1.0075	>88 090	8
	2 ^j	11.8 ^l	16 300	0	2.150	1.724	1.0200	>81 544	9

^a Pressure at fast fracture, attempts at fast fracture and failure.^b σ_h = hoop stress normal to crack = $1165P + 0.597N_x$ for panel 15 and $1383P + 0.9714N_x$ for panel 16.^c σ_x = axial stress parallel to crack = $8.4N_x + 121P$ for panel 15.^d Crack length at fast fracture, attempts at fast fracture or failure.^e σ_{RC} = gross calculated hoop stress at failure.^f Reference Table 1.^g One-bay crack.^h Two-bay crack with center frame intact.ⁱ Two-bay crack with center frame intact and center crack stopper cut.^j Two-bay crack with both center frame and crack stopper cut.^k Maximum pressure applied without fast fracture.^l Failure occurred due to outer crack stopper failure.

were arrested at the frames. It can be seen that the value of K_c^* is increased effectively by 8 percent when an axial stress of 2500 psi is present and 23 percent with an axial stress of 28,495 psi. Axial compressive stress parallel to the crack, which normally causes buckling, is minimized by axial tensile stress and would be cancelled out entirely in the case of test 4. Figure 23 shows the crack arrested between rivets after test 1 of panel 15.

The crack stopper was saw cut completely and a cut was made in the skin in a longitudinal direction on panel 16. Cyclic loading was applied to propagate the crack and several attempts were made at various crack lengths to cause fast fracture. The value of K_c^* listed in Table 11 for test 1 on panel 16 is the maximum stress intensity applied without fast fracture at the most critical crack length. The center frame was cut completely for test 2 and the skin crack extended to 43 in. in length. Failure occurred at 11.8-psi pressure as a result of outer crack stopper failure. Just prior to failure, the stress intensity in the skin was as listed for K_c^* during test 2. Analysis case 9 of Table 2 predicts a crack stopper stress of 183,000 psi with total crack length of 43 in. and gross stress of 16,300 psi. Typical values of F_{tu} from coupon tests go as high as 167,000 psi for titanium 8-1-1 so that the analysis was 10 percent conservative.

A two-bay circumferential crack test with a broken central longeron was conducted on panel 16. The equations governing the skin and longeron axial stresses, accounting for Poisson's ratio effects [15], are

$$\sigma_{skin} = 11.25 N_x + 126.8P$$

$$\sigma_{long} = 11.88 N_x - 298.6P$$

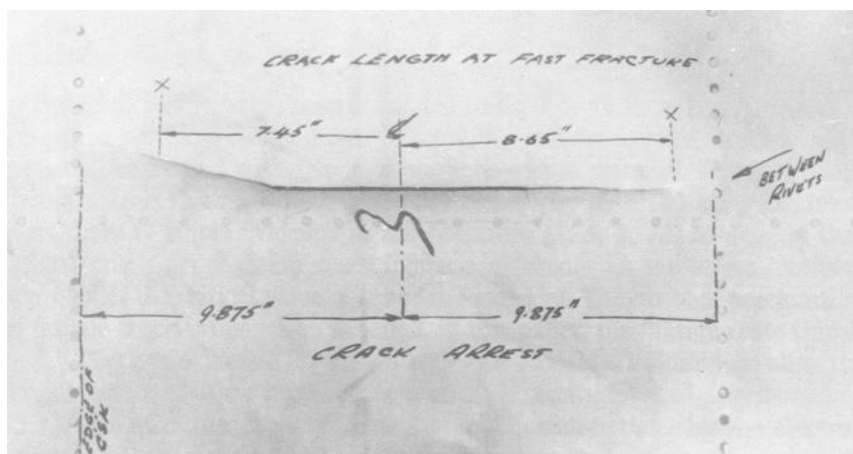


FIG. 23—View of panel 15 showing arrest of one-bay crack.

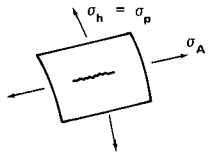
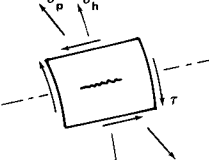
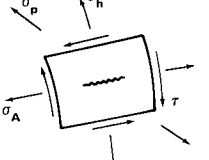
A		$\sigma_p = \sigma_h$
B		$\sigma_p = \frac{\sigma_h}{2} + \left[\left(\frac{\sigma_h}{2} \right)^2 + \tau^2 \right]^{1/2}$
C		$\sigma_p = \frac{\sigma_h + \sigma_A}{2} + \left[\left(\frac{\sigma_h - \sigma_A}{2} \right)^2 + \tau^2 \right]^{1/2}$

FIG. 24—Principal stress equations for cases A, B, and C.

Several attempts were made at total crack lengths up to 16.0 in. to cause fast fracture with an axial load $N_x = 2420$ lb/in. and a pressure $P = 9.1$ psi. Skin stress was 28,380 psi and longeron stress 23,600 psi. The maximum value of K_{e^*} , determined without fast fracture, was $>131,700$ psi $\sqrt{\text{in}}$. During this test it was not intended to fail the panel but merely to show a static capability to carry an axial skin stress of 28,380 psi with a broken longeron and two bays of skin cracked.

Unstiffened Cylinders

The prime purpose of this series of tests was to investigate the effects of shear combined with pressure on the residual strength of a cracked cylinder. The intention was to determine if the gross principal stress at failure, calculated from condition C of Fig. 24, could be compared to the gross allowable stress obtained from condition A. As the presence of the biaxial tension stress σ_A improves the gross strength by cancelling some of the compression stress parallel to the crack edge, it would be more reasonable to determine the principal stress from condition B, neglecting the axial stress σ_A . The terms appearing in Fig. 24 are defined as follows:

- σ_h Hoop stress, psi
- σ_A Axial stress, psi
- τ Shear stress, psi
- σ_p Principal stress, psi

The results of the tests are shown in Table 12 and plotted in Fig. 25. It can be seen by comparing the results of the first six cylinders in Table 7 that the presence of shear reduces the gross residual strength. Comparing principal stress at failure of cylinders with applied shear to the allowables for cylinders without shear is conservative; however, the calculation of principal stress, neglecting axial stress (as in case *B* of Fig. 24), gives a closer approximation to condition *A* than the calculation of principal stress from condition *C*.

Rivet Shear Deflection Test Results

In order to verify the rivet deflection (Eqs 3 and 5) for titanium and aluminum, several small tests were performed on lap splice specimens. Each specimen consisted of a strip of 6Al-4V single annealed titanium which was riveted to a strip of 0.071-in. 2024-T3 clad sheet using RV-5197-6 countersunk rivets. The specimens were placed back to back as shown in Fig. 26 to eliminate local bending. Three thicknesses of titanium were used, 0.016, 0.020, and 0.025 in. The extension, under tensile loading, was measured over a 2-in. gage length using an extensometer. Extension of the sheet was calculated and subtracted from the overall deflection so that actual rivet deflection would be obtained. The stiffness P/δ , where P is the applied load and δ is shear deflection of the rivet (obtained from the elastic portion of the resulting load deflection curve), is compared in Fig. 26 to the value calculated from Eqs 3 and 5.

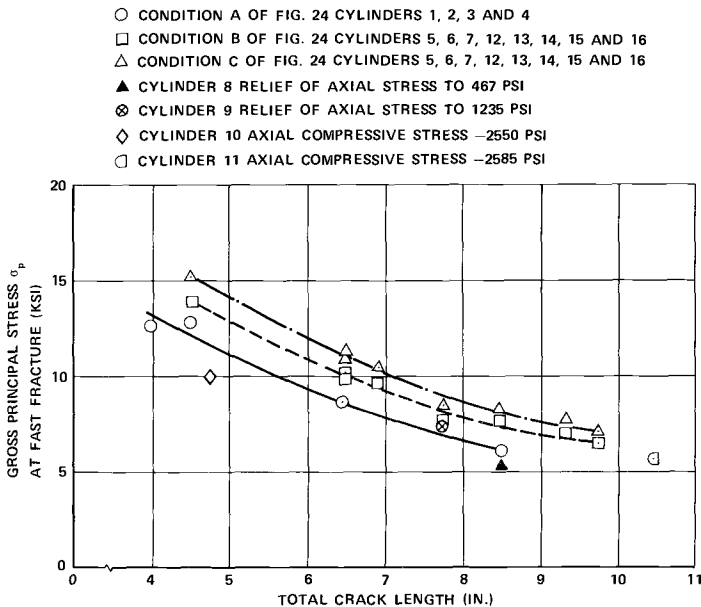


FIG. 25—Test results for 24-in.-diameter cylinder.

TABLE 12—Test results for 24-in.-diameter cylinders.

Cylinder Number	Crack Length at Failure, in.	Loads at Failure		Stresses at Failure			Maximum Principal Stress at Failure		Condition
		Pressure, psi	Torque, in.·lb	Hoop Stress, psi	Shear Stress, psi	Axial Stress, psi	Case B $\sigma_A = 0,^a$ psi	Case C Including $\sigma_A,^a$ psi	
1.....	4.00	34.0	0	12 750	0	6 275	12 750	12 750	P
2.....	4.50	34.3	0	12 880	0	6 440	12 880	12 880	P
3.....	6.44	23.0	0	8 630	0	4 315	8 630	8 630	P
4.....	8.50	16.1	0	6 030	0	3 015	6 030	6 030	P
5.....	4.50	27.3	209 250	10 250	7240	5 125	13 995	15 368	P + T
6.....	6.88	19.0	147 250	7 125	5085	3 563	9 772	10 732	P + T
7.....	8.44	15.0	116 250	5 625	4020	2 813	7 719	8 478	P + T
8.....	8.50	14.5	0	5 440	0	467	5 440	5 440	P + C
9.....	7.70	20.0	0	7 500	0	1 235	7 500	7 500	P + C
10.....	4.75	27.0	0	10 130	0	-2 550	10 130	10 130	P + C
11.....	10.50	15.0	0	5 630	0	-2 585	5 630	5 630	P + C
12.....	9.75	13.0	93 000	4 875	3210	2 435	6 468	7 089	P + T _c
13.....	7.75	15.0	117 400	5 625	4060	2 813	7 752	8 516	P + T _c
14.....	6.50	20.0	159 650	7 500	5520	3 750	10 423	11 455	P + T _c
15.....	9.313	13.85	105 090	5 190	3630	2 595	7 057	7 748	P _c + T
16.....	6.47	20.9	133 145	7 840	4600	3 920	9 964	10 880	P _c + T

Note—Condition definition:

- P = static pressure only
- P + T = static pressure + static torque
- P + C = static pressure + compression
- P + T_c = static pressure + cyclic torque
- P_c + T = cyclic pressure + static torque

^a Reference Fig. 24.

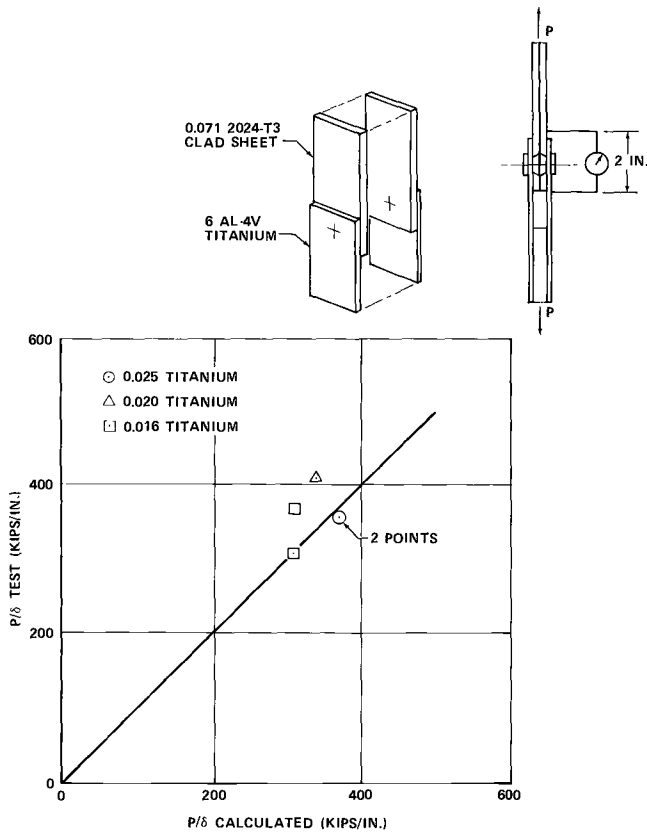


FIG. 26—Rivet shear deflection test result correlation.

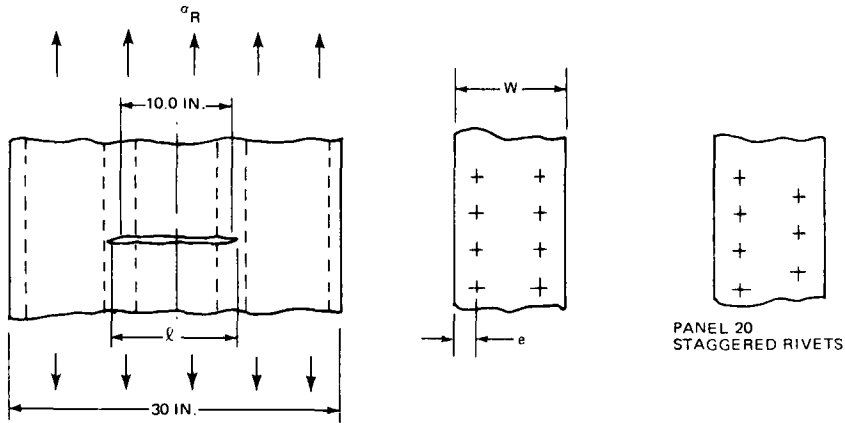
Stiffened Panels, 30 in. Wide

The test results for these panels are shown in Table 13. In all cases, the straps failed without failure of the rivets. The maximum load to be transferred to a strap in the DC-10 configuration is 4370 lb for a 42.0-in.-long crack. It can be seen from Table 13 that the value of P_c in all cases is higher than this number so that strap failure will always precede rivet failure, even with two rivet rows.

Unstiffened Panels, 30 in. Wide

Two unstiffened panels made from 0.071-in. 2024-T3 clad sheet were tested (see Fig. 27). A 9-in.-long central crack was propagated in the first panel and static load applied. Slow crack growth took place and final failure occurred at a gross stress of 24,600 psi with the crack 11.0 in. long. The second panel contained a 9-in.-long saw cut. Static load was applied and slow growth again took place to 11.0 in. before failure at the same gross stress of 24,600 psi. Antibuckling guides, set 1.0 in. apart, were used in both cases. K_c as determined for the final crack length from Eq 1 was $114,000 \text{ psi}\sqrt{\text{in.}}$

TABLE 13—Test results for 30-in-wide panels (0.071-in. 2024-T3 clad sheet titanium strap 6Al-4V).



Panel No.	W	t	e , in.	P_F , lb	l_F , in.	P_c	σ_R
17.....	2.813	0.025	11/16	89 000	11.45	5880	34 503
18.....	2.813	0.025	7/16	87 000	9.80	5725	33 727
19.....	3.438	0.020	7/8	94 000	10.50	5700	36 942
20.....	3.438	0.020	7/8	89 000	9.60	5380	34 977
21.....	4.188	0.016	1 1/16	89 000	10.60	5500	34 745
22 ^a	3.625	0.016	29/32	96 000	9.90	3060	36 185

NOTE— P_F = load at failure l_F = crack length at failure P_c = load transferred to crack stopper due to crack σ_R = gross stress at failure^a AM 350 stainless steel strap.

Rivet Shear Load Test

Figure 28 gives the results of tests performed on the small panels shown in Fig. 16g to determine the crack stopper to skin rivet shear load. A lumped parameter analysis, to determine the rivet shear load, was performed on one of the panels with a 0.020-in. strap. This analysis is used for a comparison with the results for the three thicknesses of strap. It is not expected that the strap thickness variation, in the ranges considered, will affect the calculated elastic load distribution to a high degree. The panel was divided into bars and shear panels similar to those shown in Fig. 7. The rivet loads were determined from strain gage readings on the strap. The ordinate of Figs. 28a to 28c is shown as shear flow in pounds per inch and, since the rivets are spaced 1 in. apart, this load would, therefore, be rivet load. The shear flow shown is applied to two rivets. Figure 28a shows a comparison between test and elastic analysis for a 0.025-in. strap. It can be seen that the first rivets yield at a load between 3000 and 5000 lb and more load is carried by the remaining rivets. Yielding

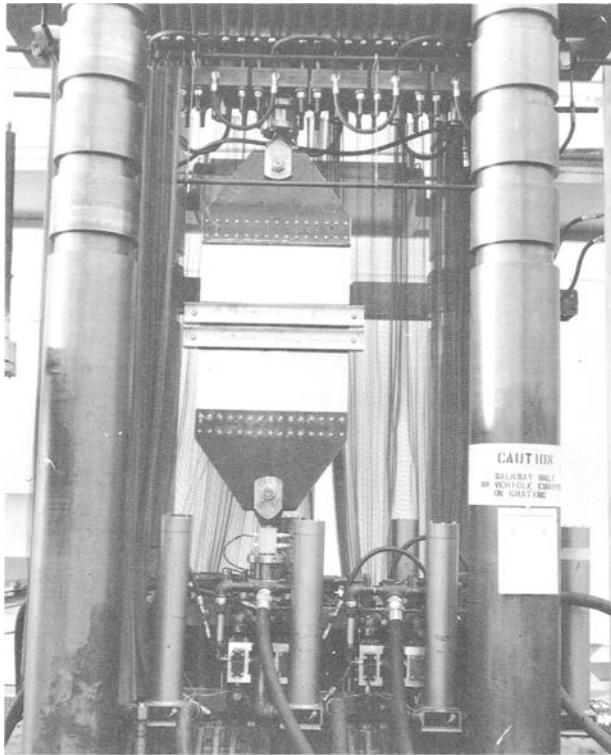


FIG. 27—Test setup for 30-in.-wide panels.

occurred early for both the 0.020 and 0.016-in. straps as shown in Figs. 28*b* and 28*c*. Figure 28*d* shows applied load versus shear load in the first rivets for tests on two panels with 0.025-in. straps. The maximum load transferred from the skin to crack stopper for DC-10 loading with a crack 42 in. long is 4370 lb. This is determined from case 6 of Table 1 with a cabin pressure of 9.2 psi and a skin stress 80 percent of PR/t hoop stress, where R is 118.5 in. It can be seen from Fig. 28*d* that little or no loss in first rivet load is experienced at this applied load. However, due to early yielding of the first rivets in the 0.020 and 0.016-in. straps shown in Figs. 28*b* and 28*c*, a loss in the crack tip stress ratio R_{ct} could be expected if 0.020 or 0.016-in.-thick straps were used.

Correlation

Skin Criteria

Space limitations prevent illustrations such as Fig. 13 for every test. Figure 29 shows the results of test 2 on panel 3. The shape of the curve is determined by analysis of case 1 of Table 1 and the height by K_c^* at fast fracture. The

curve is plotted from Eq 7. Correlation is shown with the analysis at crack arrest and final failure where the data points fall on the curve. For other tests where fast fracture, arrest, and failure occurred, the correlation is shown in the tables of test results by comparing calculated crack arrest lengths and failure stresses with those obtained from test.

Frame Criteria

An example of frame stress correlation is shown in Fig. 30 for panels 5 and 6. The other cap stresses are extremely close to the analysis but the inner cap stresses are lower. This kind of correlation is typical of all the tests performed. The outer, more critical cap stresses were always extremely close to the analysis results.

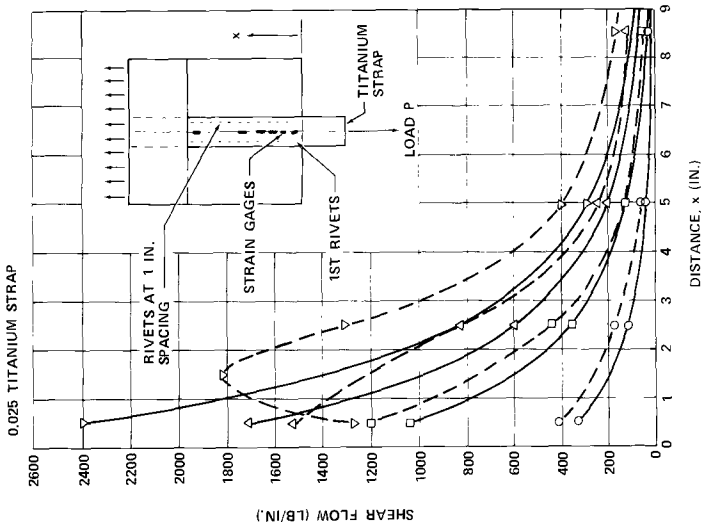
Longeron Criteria

Longeron bending stresses were not predicted accurately on any of the tests on flat panels 7 to 14. Secondary effects due to center longeron bending influenced the test results. Figure 31 shows that at some distance from the crack the longeron load P is acting at the centroid of the section. This load is reacted to eventually by the skin ahead of the crack and is thus transferred a distance e , which causes the longeron to bend inwards. The induced bending in the center longeron for a uniaxial loading case causes the outer longerons to be loaded as shown in Fig. 31b. The resultant bending in the outer longerons tends to cancel out the bending caused by transfer of load from the cracked skin as indicated in Table 4. The load input to the longeron, however, is accurately predicted by the analysis for the flat panels as illustrated by Fig. 32 for panels 8 and 12. If the panel section shown in Fig. 31b were a section of a pressurized shell, then the inward bending of the center longeron would be relieved by the cabin pressure and the loading W' , causing relief to the outer longeron bending, would not be present. This is illustrated by Fig. 33, which shows outer longeron stress correlation for the circumferential crack test on panel 16. It can be seen that the analysis accurately predicts the longeron stress for the pressurized panel; also, that testing flat panels to determine fail-safe allowable stresses for curved panels under pressure for this condition should be treated with caution, particularly if the residual strength is determined by stiffener criteria. The relief due to longeron bending will produce allowable stresses higher than would be obtained from a curved panel test.

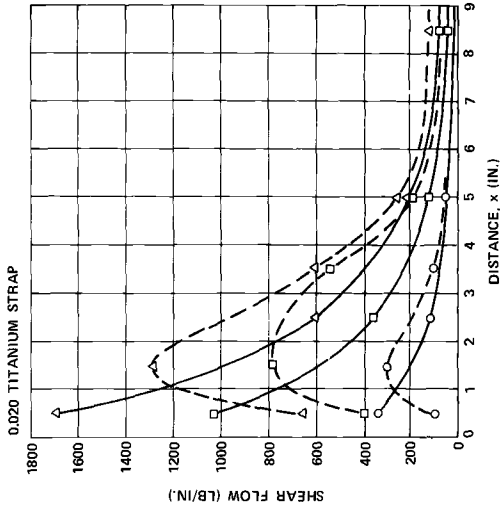
Final Configuration Selection

The test results of the 24-in.-diameter cylinders, although qualitative due to their comparatively diminutive size, do at least indicate that shear stresses reduce the residual strength in the presence of fatigue cracks. Figure 25 indicates that principal stresses determined from condition *B* of Fig. 24 are slightly conservative when compared to the allowables determined from condition *A*. It was decided to account for shear by comparing the results for

P (LB)	CALCULATED	TEST
1000	○ — ○	○ — ○
3000	□ — □	□ — □
5000	△ — △	△ — △
7000	▽ — ▽	▽ — ▽



P (LB)	CALCULATED	TEST
1000	○ — ○	○ — ○
3000	□ — □	□ — □
5000	△ — △	△ — △



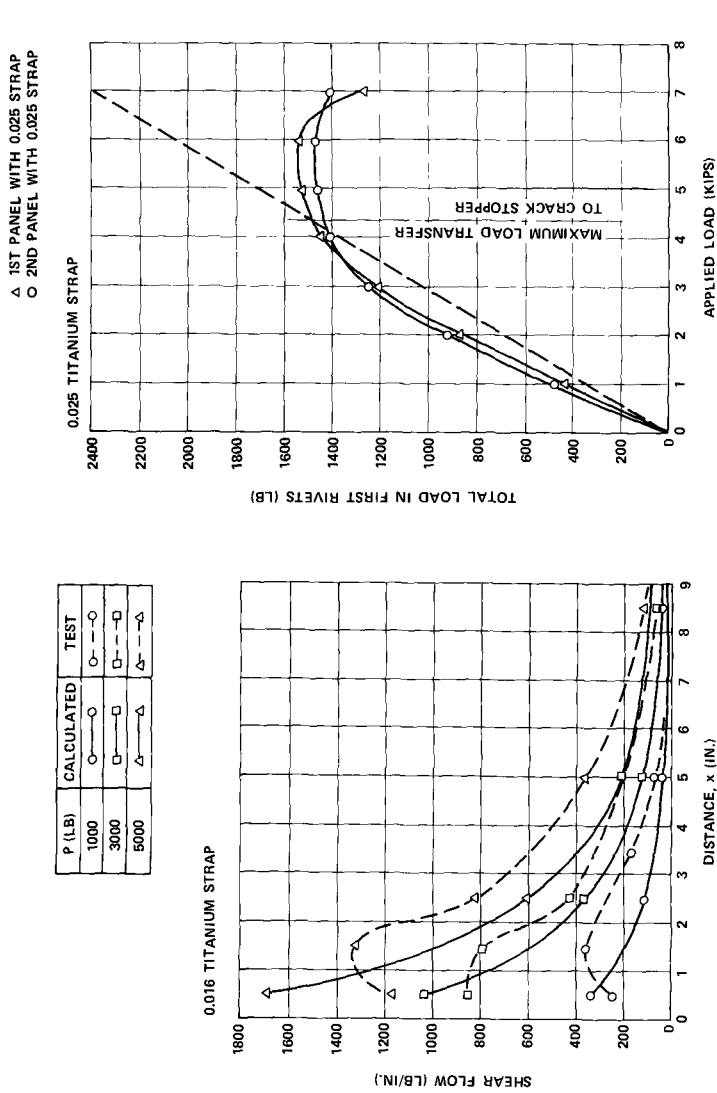


FIG. 28—Rivet shear load—analysis, test correlation: (a) 0.025, (b) 0.020, (c) 0.016, and (d) 0.025-in. titanium strap.

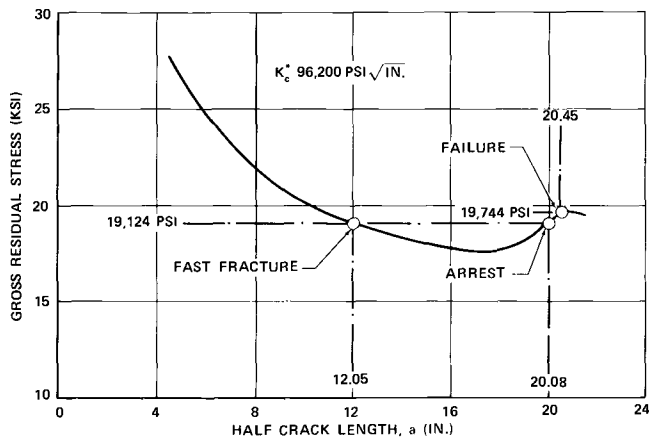


FIG. 29—Gross residual strength curve, test 2, panel 3.

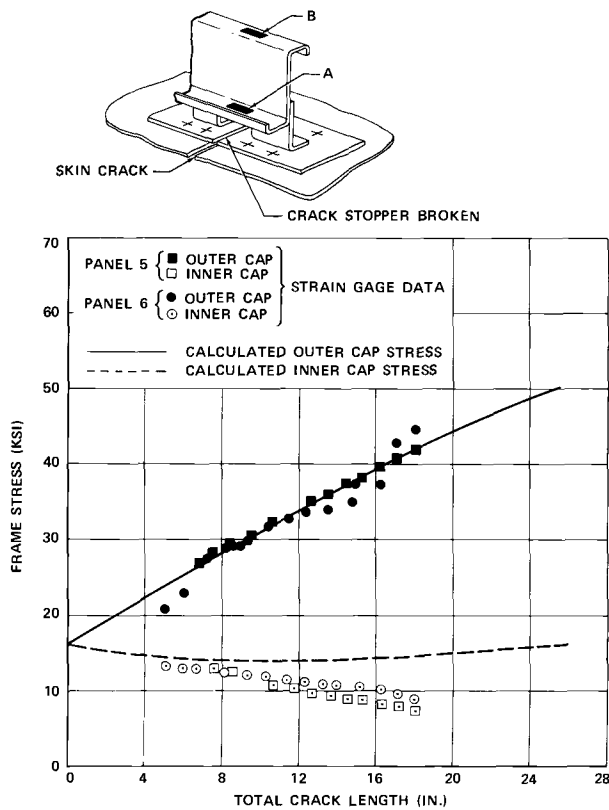


FIG. 30—Center frame stress correlation two-bay crack test, panels 5 and 6, test 2; gross stress, 16,400 psi.

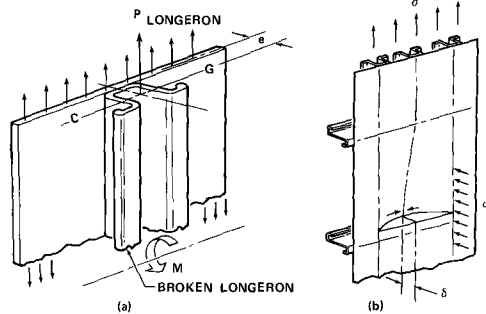


FIG. 31—Center longeron bending.

panels symmetrically loaded to a principal stress determined from condition *B* of Fig. 24 which neglects axial stress. The effects of axial tension increase the allowable stress, as seen from the results of tests 2 and 4 of panel 15 listed in Table 11.

Longitudinal Cracks

The highest limit design principal stress in the minimum gage portion of the shell is approximately 19,000 psi from hoop stress and shear. It was desirable to show that the structure was fail-safe for limit values to satisfy foreign requirements. The gross residual strength from flat panels 2, 3, and 4 without crack stoppers and with 7075-T73 skin range from 18,100 to 19,744 psi as listed in Table 8. The various shear clips on these panels shown in Table 5

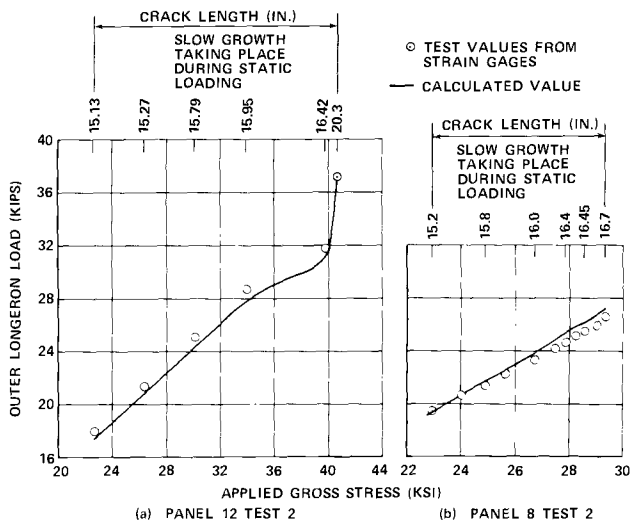


FIG. 32—Outer longeron load, flat panel with circumferential crack.

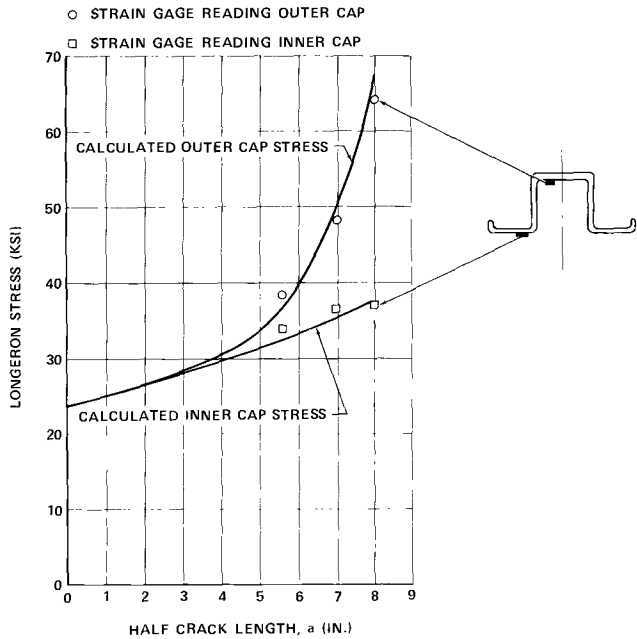


FIG. 33—Outer longeron stress correlation circumferential crack test, panel 16.

and illustrated in Fig. 3 do not vary the strength significantly. The results of tests on curved panel 15 indicate a 30 percent loss in strength due to bulging from pressure. This is indicated by K_e^* values from flat panels listed in Table 8, compared to those for curved panel 15 for tests without axial load listed in Table 11. It can be seen that 7075-T73 skin on panels without crack stoppers would, at best, only produce an allowable gross stress of 13,800 psi. With 2024-T3 skin without crack stoppers, using R_{ct} for $a = 21.5$ of 1.81 (from case 1 of Table 2) and a K_e^* of 88,090 $\text{psi}\sqrt{\text{in.}}$ (from Table 11), the gross allowable stress is just a little over 19,000 psi. In view of this, it was decided to use both 2024-T3 skin, 0.071 in. thick, and crack stopper straps for the minimum gage portions of the shell. Test 2 on panel 5 listed in Table 8 had indicated that a gross stress of 25,118 psi could be applied without failure of the crack stopper to skin rivets. It was decided, therefore, to use only two rows of rivets, since the load transfer into the crack stopper would only be based on a gross stress from hoop tension in the region of 12,000 psi. Tests on 30-in.-wide panels listed in Table 13 had indicated that the required load could be transferred to the crack stopper with two rows of rivets. Reducing the crack stopper thickness from 0.025 in. was considered, but tests on panels shown in Fig. 16g, with results plotted on Figs. 28a to 28c, indicated that the first rivets yield early on all thicknesses other than 0.025 in. Figure

28d shows that adequate load can be transferred before rivet yield. The gross residual strength of this configuration is approximately 26,000 psi using R_{ct} from case 6 of Table 2. Titanium was chosen for crack stopper material because of its high strength to weight ratio and resistance to fatigue, which ensures skin cracking before crack stopper cracking.

Circumferential Cracks

2024-T3 material had been chosen for the longitudinal crack case. This choice was substantiated by tests on 2024-T3 panels 11 to 14 of Table 10 compared to 7075-T73 panels 7 to 10 of Table 9. K_{c}^* values are shown to be almost double those of 7075-T73. Comparing allowables for the same longeron, for example, panel 8, using 7075-T73, failed at 29,600 psi (Table 9). Panel 12 with a similar longeron but with 2024-T3 skin failed at 40,855 psi. Hat-section longerons, in conjunction with 2024-T3, were therefore chosen for the circumferential crack condition. This configuration gives more than adequate fail-safe capability for the selected damage tolerance.

References

- [1] Stone, M., "Structural Reliability Through Detail Design and Development Testing," Air Force Conference on Fatigue and Fracture of Aircraft Structures and Materials, Miami, Fla., 15-18 Dec. 1969.
- [2] Wang, D. Y., "An Investigation on Fatigue Crack Propagation and Fail-safe Design of Stiffened Large Aluminum Alloy Panels with Various Crack Stoppers," Proceedings, 10th ASME/AIAA Structures, Structural Dynamics and Materials Conference, New Orleans, La., April 1969.
- [3] "Crack Propagation Prediction and Crack Stopper Techniques for Stiffened and Unstiffened Flat Sheet in a Supersonic Environment," ASD-TDR-63-773, Douglas Aircraft Co., Inc., Long Beach, Calif., Sept. 1963.
- [4] Hunt, R. T., "Residual Strength and Crack Propagation in Stiffened Panels," Douglas Report LB 31837, Douglas Aircraft Co., Inc., Long Beach, Calif., Nov. 1964.
- [5] Eide, G. R., "Fail-safe Design of Stiffened Panels," Douglas Report LB 32056, Douglas Aircraft Co., Inc., Long Beach, Calif., Dec. 1964.
- [6] Irwin, G. R., *Journal of Applied Mechanics*, JAMCA, Vol. 24, Sept. 1957, p. 361.
- [7] Allen, F. C., "Stress Analysis of Centrally Cracked Plates," presented to ASTM Committee E-24, March 1969.
- [8] Denke, P. H., "A General Digital Computer Analysis of Statically Indeterminate Structures," Douglas Paper 834, Douglas Aircraft Co., Inc., Long Beach, Calif., Sept. 1959.
- [9] Denke, P. H., "A Computerized Static and Dynamic Structural Analysis System; Part III. Engineering Aspects and Mathematical Formulation of the Problem," Douglas Paper 3123, presented to the SAE International Automotive Congress and Exposition, Jan. 1965.
- [10] Picard, J. and Morris, R. C., "Format 11—Second Version of Fortran Matrix Abstraction Technique," AFFDL-TR-66-207, Vols. I and III, Douglas Aircraft Co., Inc., Long Beach, Calif., Dec. 1966.
- [11] Swift, T. and Wang, D. Y., "Damage Tolerant Design-Analysis Methods and Test Verification of Fuselage Structure," presented to Air Force Conference on Fatigue and Fracture of Aircraft Structures and Materials, Miami, Fla., 15-18 Dec. 1969.
- [12] Westergaard, H. M., *Journal of Applied Mechanics*, JAMCA, Vol. 6, No. 1, June 1939, p. A49.

- [13] Liu, A. F., "Statistical Variation in Fracture Toughness Data of Airframe Materials," presented to Air Force Conference on Fatigue and Fracture of Aircraft Structures and Materials, Miami, Fla., 15-18 Dec. 1969.
- [14] Broek, D., "The Residual Strength of Aluminum Alloy Sheet Specimens Containing Fatigue Cracks or Saw Cuts," C.C.L. Class G 311: G 331, Report NLR-TR M.2143, National Lucht—En Ruimtevaartlaboratorium, National Aero Space Laboratory, NRL Amsterdam.
- [15] Flugge, W., "Stress Problems in Pressurized Cabins," NACA T.N. 2612, Stanford University, Feb. 1952.